LITHEUM. A Web-based Lighting and Thermal Urban Model for City Energy Assessment

1.Introduction

Urban areas and their associated activities are responsible for 75% of the carbon emissions and 80% of the energy consumption worldwide (Keirstead, 2013). The operation of the building stock accounts for approximately 25% of energy consumption and 17.5% of global greenhouse gas (GHG) emissions (Ritchie, 2020). Consequently, to achieve a meaningful impact and meet the objectives of the Paris Agreement, strategies for mitigating climate change must address existing buildings. The European Commission has defined a long-term strategy to accelerate building renovation: the Renovation Wave Strategy (European Commission, 2020). One of the objectives of this action plan is to optimize the environmental returns of investments. The plan targets and prioritizes buildings with high heating and cooling demands. Although the EU member states of the European Union are responsible for the transposition of the Renovation Wave Strategy at the national level, the implementation of detailed plans is typically undertaken at the municipal level. The allocation of financial resources is determined by local councils, which select specific areas and neighbourhoods for funding (Rodríguez-Álvarez, 2023). Nevertheless, the administrations lack a decision support tool that would enable them to obtain meaningful information about the energy performance of existing urban areas. This is particularly problematic in terms of the potential energy savings from renovation policies.

Despite the fact that energy building modelling has become a common standard in the construction sector following the implementation of the Energy Performance of Buildings Directive (EPBD) (DEA, 2018), the existing tools are not intended for large urban areas.

Existing tools are not intended for large urban areas. As Mendes et al. ((Mendes et al., 2024) pointed out that the acquisition of meaningful results is contingent upon the provision of detailed inputs for each thermal zone. The primary obstacles to the implementation of such detailed models at the urban scale can be categorised as follows: firstly, the absence of detailed building information to define the input parameters. (Chen et al., 2017); secondly, the lack of measured energy data to calibrate the model (Kamel, 2022); and thirdly, the substantial computational capacity that is required (Dogan & Reinhart, 2017).

The development of Urban Building Energy Models (UBEM) as a scientific field has been described as a gradual evolution that began in the 1990s and continued into the 2000s (Salvalai et al., 2024). The initial explorations were mostly statistical models devoid of spatial inputs (e.g. Hirst, 1978; Jones & Lannon, 1998). The paucity of data and the limited implementation of Geographic Information Systems (GIS) acted as constraints (Swan & Ugursal, 2009). The subsequent generation of UBEM integrated user application interfaces is intended to facilitate their integration into planning processes. The LT-Urban was one of the first attemps to calculate urban energy demand conducted in an architectural environment (Ratti et al., 2000). The SuntTool integrated different resource flows (energy, water and waste) for new urban projects using a thermodynamic approach (Robinson et al., 2007). This project was followed by CitySim (Robinson, 2011), which introduced GIS for data processing and a stronger focus on energy. Following the transposition of the EPBD to Spain, a simple thermal model was developed to calculate the energy demand in small urban areas (Turégano & Hernández, 2008) and a UK Consortium led by the Building Research Establishment worked on Climate Lite, a CAD-like application that build off the LT model to develop an early stage simulation

tool (BRE, 2009). Although these examples were not widely implemented they sowed the seeds for subsequent projects.

There has been a strong acceleration in the UBEM field from 2010. One of the key drivers of this surge has been interoperability, which has facilitated the integration of well-tested thermodynamic models through the development of modular and flexible codes. Some representative examples combined existing CAD and GIS environments with thermodynamic models to speed up the geometric definition process. The Urban Modelling Interface (UMI) (C. Reinhart et al., 2013) developed an API that connects 3DRhino to a SQLite database containing the thermal and lighting information. URBANopt uses EnergyPlus and OpenStudio to analyse city blocks and districts (El Kontar et al., 2020). The initial version of City Energy Analyst integrated the simple hourly dynamic method of EN 13790 with GIS (Fonseca & Schlueter, 2015). Its modular structure allowed later integrations with daylighting (Jimeno Fonseca et al., 2024) and microclimatic simulation tools (Maiullari et al., 2018). These models are representative of UBEM for expert users, optimised for the assessment of new developments and intermediate scales (several urban blocks or a small neighbourhood). Web-based applications have recently gained traction due to improved internet quality and connectivity, and the development of JavaScript libraries that can translate analytical algorithms (e.g. Three.js, Leaflet, etc...). Most online urban energy applications are static maps (e.g. London Heat Map, New York Energy & Water Performance Map). UBEM.IO is a web-based application that prepares GIS data for subsequent energy modelling using a combined approach of desktop and online processing (Ang et al., 2022; Rodríguez-Álvarez & Alvaredo-López, 2023).

Recent reviews of UBEM have classified them based on their approach to the urban scale and the energy calculation method (Ferrando et al., 2020; C. F. Reinhart & Cerezo Davila,

2016; Swan & Ugursal, 2009) . In terms of urban form characterisation, they can follow a top-down approach, aggregating multiple buildings, or a bottom-up perspective, analysing buildings individually. In terms of energy calculations, the UBEM literature distinguishes between two main classes: thermodynamic models, usually referred to as "white box" models, and statistical models, also referred to as "black box" or "data driven" models. The former apply formulas from building physics, while the latter use measured data to derive energy estimates by applying statistical techniques (Aerts et al., 2014; Richardson et al., 2008). A third approach combines physics with statistical methods to create hybrid models, thus adapting the number of input parameters to the available data. They use different techniques and assumptions to integrate the contributing factors that drive energy demand in buildings (Hong et al., 2020). The thermal characteristics of the building stock are often assumed based on certain proxies, such as construction date, typology and location, due to the lack of datasets containing this information. The European standard EN 16798-1 has defined hourly occupancy schedules for energy calculations in residential buildings to meet the requirements of the EPBD (Ahmed et al., 2017). The digitisation of building logbooks is a recent initiative aimed at overcoming the data gap (Gómez-Gil et al., 2023).

This paper reports on the research and development of a Lighting and Thermal Urban Model (Litheum), which takes a user-centred approach to combine interactivity and computational optimisation, allowing its integration as a web application. The user interface is an interactive map of the city showing energy demand for heating, cooling and lighting. Users can select buildings or urban areas to create alternative scenarios based on common building energy conservation measures (i.e. insulation and window upgrades). The expected energy savings are visualised in the map as well as in hourly and monthly graphs. The parameters of the initial map were previously calculated and stored

in a database, which is linked to the energy modules to update its values each time a new scenario is created. A hybrid UBEM model has been developed based on original algorithms to extract the relevant parameters for the energy analysis, and also incorporates methods defined in EN 52016 for thermal calculations. The BRE daylight factor method (BRE, 1986) and the lighting model defined in the precedent UEIB (Rodríguez-Álvarez, 2016) were used to estimate the lighting loads. Both lighting and thermal models calculate the expected demand of urban buildings based on the construction and spatial characteristics, leaving aside the efficiency of the systems, which would introduce an additional degree of uncertainty. This article focuses mainly on the definition and validation of the thermal model.

2. Materials and Methods

2.1 Data preparation workflow

The web application enables the user to identify the energy demand, disaggregated into the heating, cooling, and lighting of a city or an urban area. Furthermore, it facilitates the recalculation of demand post-introduction of alternative scenarios grounded in energy conservation measures, including wall and roof insulation, or window replacement. In addition to the energy demand data, the user has the capacity to obtain the monthly energy balance and hourly temperature graphs for a selected building. The application facilitates the download of calculated data in tabular or graphical form, and its subsequent visualisation on maps.

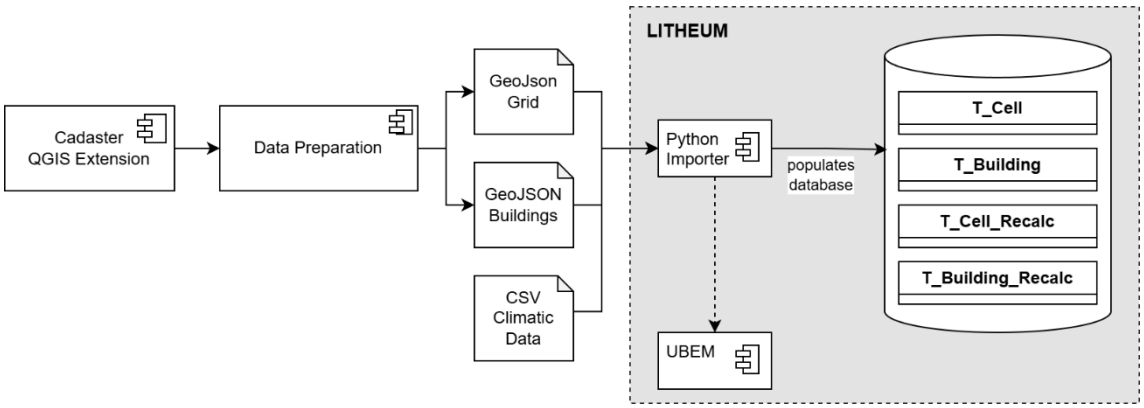

Fig. 1 Data preparation workflow

As illustrated in *Fig. 1* , the workflow has been designed to facilitate the populating of the database that stores the relevant building information on the server. The following steps are required: Firstly, the cadastral cartography is obtained using the QGIS plugin Spanish Inspire Cadastral Downloader(Soriano et al., 2024). A comprehensive set of critical building parameters is determined for each building, encompassing parameters such as the obstruction angle in various orientations and the area of the exposed envelope, amongst others. Furthermore, an analytical grid is created to overlay the entire city area, and the average building parameters are computed for each cell in the grid. The grid retains information on all key parameters regarding energy calculations. This is in accordance with the approach proposed in the precedent method, the Urban Energy Index for Buildings (UEIb) (Rodríguez-Álvarez, 2016).

Following the preliminary processing stage, two vector layers are obtained: the grid layer and the building layer. The files are exported as GeoJSON, facilitating straightforward retrieval by the energy model and the PostgreSQL database. The input and output parameters contained in these files are explained in detail in Appendix A. The process results in two GeoJSON files: one containing the grid data and another with disaggregated data for each building. Finally, the climatic data is incorporated into the source files, with

the files being formatted in CSV (Comma Separated Values) format. Subsequent to the assembly of the three source files, the process is entirely automated. The files are processed through a Python importer, which populates a database storing all the data about cells and buildings in two tables that contain the baseline scenario: "t_cell" and "t_building". A component, referred to as "UBEM" in *Fig. 1*, implements the UBEM for the Litheum platform. Two additional tables are created (t_cell_recalc and t_building_recalc) for the purpose of storing data whenever a new scenario is defined by the user and the energy demand is recalculated. In this particular instance, the web application employs the same component ("UBEM" in *Fig. 1*). to ascertain the new demand in accordance with the energy conservation measures that have been implemented.

2.2 Data sources

The morphological characteristics, climatic data, and the thermophysical parameters are obtained from the following sources using bespoke modules for automatic processing:

The morphological attributes are obtained by exploiting the Spanish cadastral database, which includes spatial and alphanumerical information for the majority of the territory (SEC, 2024). The spatial data is available in vector format (shapefile) and classified by municipalities and categories (parcels, buildings, sub-buildings, addresses…). The tables of attributes contained within the shapefiles provide a basic overview of the available information, including the Cadastral Reference ID and the building height. Further data associated with each feature can be obtained by downloading additional tables. These supplementary files, designated CAT, should be processed separately from CSV files. These documents contain pertinent information regarding the utilisation of the structure, its construction date, any subsequent renovations (if applicable), the current state of conservation, and its total built-up area (SEC, 2024). The cadastral cartography is intended for GIS and is subject to constant updating and maintenance, in accordance with

rigorous quality control procedures (García Cepeda, 2006). However, the presence of erroneous values and anomalies, including incorrect heights or uses, necessitates the filtration of the data prior to further processing. The Spanish Inspire Cadastral Downloader plugin for QGIS facilitates the establishment of the requisite connections between the shapefiles and the CAT files by employing the ATOM Syndication Format in accordance with the INSPIRE Directive (Soriano et al., 2024).

The acquisition of climatic data for any given location is facilitated by the Photovoltaic Geographical Information System (PVGIS). It is a web-based application that provides hourly data on various meteorological parameters, including solar radiation, air pressure, wind velocity, humidity, long-wave radiation, and temperature. It covers most regions worldwide (EU Science Hub, 2024). In this project, the dataset is downloaded in the form of a Typical Meteorological Year (TMY) format, stored in a CSV file. In order to feed the energy model, it is necessary to obtain hourly vertical direct and diffuse solar radiation in, at least, the four main orientations, as well as the horizontal radiation and sun position (altitude and azimuth). The transformation templates provided by EN ISO 52010 are used to obtain these values (van Dijk, 2021).

In terms of the thermophysical properties of the buildings, the classification and methodology proposed in the study to estimate the domestic heating demand as part of the Long Term Renovation Strategy (LTRS) of the Spanish government (Arcas Abella et al., 2018) was followed. In this study, the building stock is classified into 15 typological clusters, following a combinatorial matrix of three parameters: building age, height and number of households. The classification system is divided into five categories based on the date of construction: before 1940, 1941-1960, 1961-1980, 1981-2007 and after 2007. These dates are associated with new building regulations or technologies, which are reflected in the typical thermal transmittance of the building elements. The LTRS defines

the U-values for walls, windows, roof and floor, as well as infiltration values associated with each period (see *Table 1*). The Litheum model applies these values to calculate the current thermal performance of existing buildings. The transmittance table is updated in accordance with the implementation of energy conservation measures as defined by the user.

Table 1 U-Thermophysical building properties according to year of construction

	U-value (W/m2K)				Infiltration
Year	**Floor**	**Wall**	**Roof**	**Window**	**(ACH)**
<= 1940	1.15	2.12	2.21	4.24	1.5
1941-1960	1.15	2.08	2.21	4.24	1.3
1961-1980	1.15	1.5	1.7	4.24	1.1
1981-2007	1.06	1.5	1.4	3.1	0.9
>= 2008	0.62	0.74	0.46	2.9	0.63

**ACH assumes natural conditions*

2.3 Web application

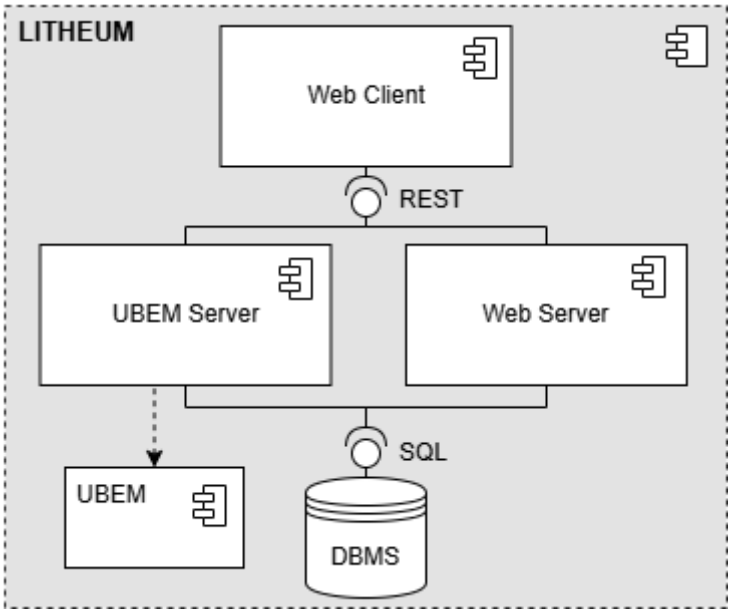

Fig. 2 Architecture of the web platform to display the Litheum energy maps

The software architecture of the web application is shown in Fig. 2. The database (DBMS) which is populated through the previously described workflow, is illustrated at the bottom

of the figure. The implementation of the system is facilitated by PostgreSQL, a robust and open-source relational database management system that offers substantial support for data integrity, complex queries, and concurrent user access (PostgreSQL Global Development Group, 2024). In order to extend the capabilities of the system with regard to the handling of spatial data, the PostGIS extension is utilised. PostGIS augments the functionality of PostgreSQL by incorporating geographic object support, thereby facilitating the efficient storage, querying, and analysis of spatial data. The backend functionality of the database is divided into two web server applications. The UBEM Server is a web server developed in Flask (*Flask*, 2024) that encapsulates the UBEM Python module and provides endpoints to use specific calculations related to the UBEM. The Web Server has been built on the Spring Framework (*Spring Framework*, 2024), fulfils typical web functions such as database interaction and client data request management. These include the retrieval of data for the purpose of displaying charts, as well as the management of user interactions with the map interface, such as zooming, panning, and the selection of specific areas of interest. These functions in turn initiate the retrieval of relevant data for further analysis and visualisation. The top layer is populated by a web client developed using Vue.js (You, 2024), which provides the user interface and integrates both servers to deliver the platform's functionalities.

The primary objective of the web application is to visualize, access to and querying of the heating, cooling and lighting demand from the building stock. The two principal features of the system are data visualisation and data simulation.

The platform provides vector-based visualisation capabilities. Each feature displayed on the map is characterised by a distinct geometry, which is not represented as an image (or raster tile). It enhances the user experience by facilitating interactivity with all the elements. However, this approach often entails large computing resources (i.e. processing

hundreds of elements instead of a single image). In order to address this issue, the map employs a grid-based representation for extensive regions, thereby aggregating the energy consumption of each area within a single cell. The building geometries are displayed as the user zooms in. Moreover, both visual modes (grid and building) retrieve only the features that are within the screen's bounding box. Consequently, the system does not have to retrieve and draw any geometry that is beyond the view.

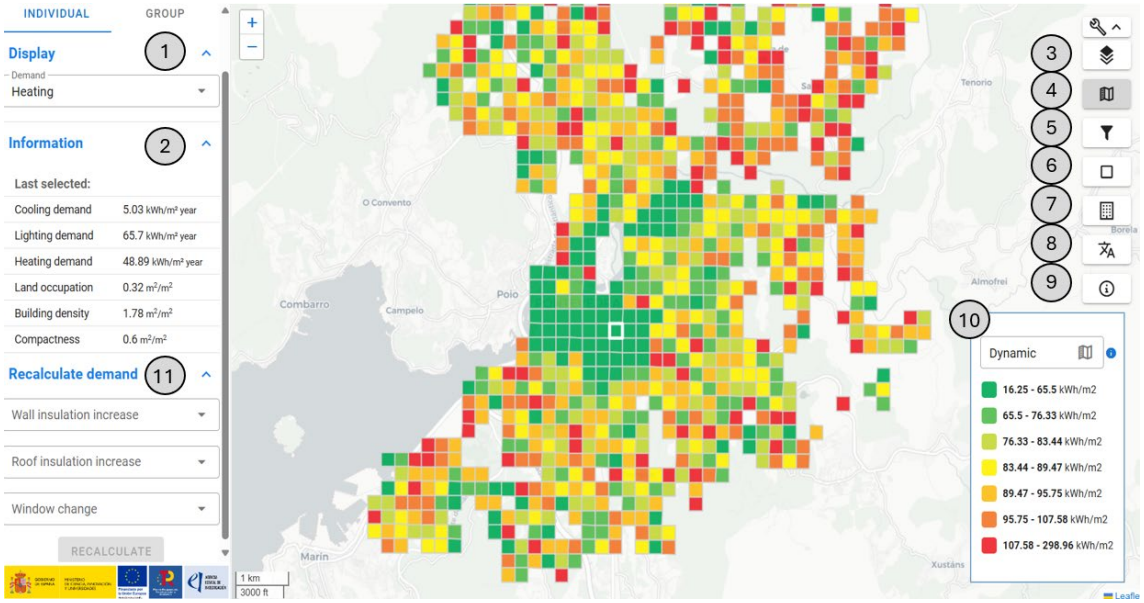

Fig. 3 Main interface of the web application

As illustrated in Fig. 3, whilst utilising the platform, the majority of the screen is dedicated to the map. The following example illustrates the grid mode over the municipality of Pontevedra (Spain), whereby the information regarding building demand (1) is grouped based on the colour palette (10) shown in the legend. Should a cell be selected (highlighted in the figure), detailed information pertaining to that specific zone will appear on the left panel (2). This will include not only demand data, but also information regarding land occupation and building density. The buttons located on the right of the screen offer a range of customisation options, including the basemap layer (3), the legend (4), the display or concealment of the floating left menu (5), the polygon selector (6), the selection of individual buildings rather than cells (7), the language (8) and the general

information menu (9). For instance, the initial adaptation of the legend classes to EPC classification is in accordance with the Spanish Code. However, modification of the legend classes is possible, with the result that they automatically fit the range of values displayed on the screen. **Fig. 4** shows another screenshot of the application, displaying the building visual mode.

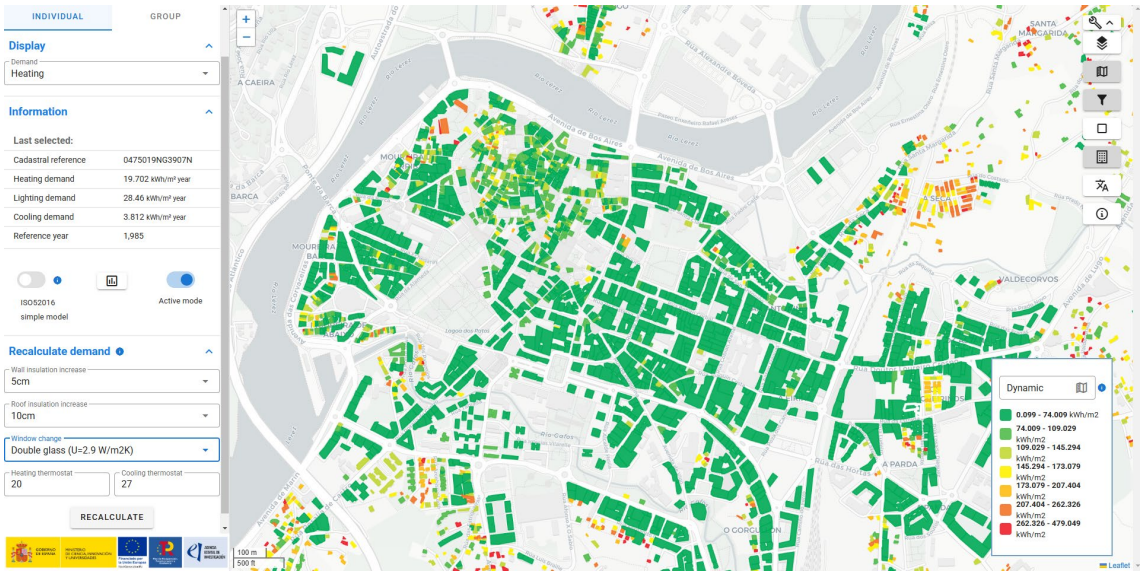

Fig. 4 Main interface of the web application showing the *building* visualization mode

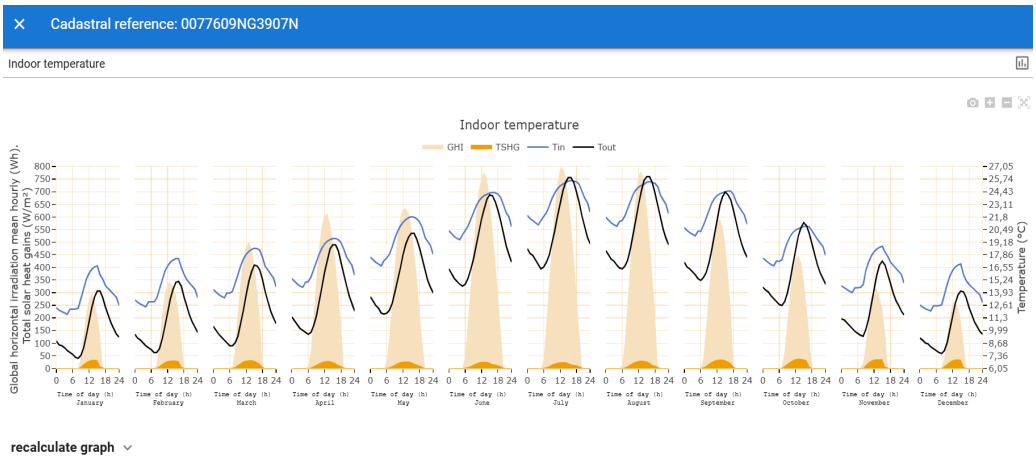

Fig. 5 Energy balance (top) and Indoor temperature (bottom) for selected buildings

The web application generates charts for individual buildings, which represent the energy balance and the hourly indoor temperature (**Fig.** *5*). The energy balance shows the monthly fluctuations and break down in heat gain and loss. The temperature graph is a visual representation of the mean hourly values for indoor and outdoor temperatures, internal solar gains and global solar gains for each month.

2.3.1 Definition and assessment of alternative scenarios

The pre-calculated heating, cooling and lighting loads are stored in the base layer of the main spatial database, which is stored in a central server. It is then possible for users to modify parameters associated with insulation, thermostats, ventilation and windows. This process enables the definition and evaluation of alternative energy conservation measures. The recalculation demand dialog of the application provides three initial energy conservation measures when the visualization mode is the analytic grid, with various options within each measure (Fig. 3, object 11):

- Wall insulation, with options “No additional insulation”, and additional 5 cm, 10 cm or 15 cm of insulation thickness.

- Roof insulation: with options “No additional insulation”, and additional 10 cm or 20 cm of insulation thickness.
- Window replacement, with options “No changes”, standard double glazing window (U=2.9 W/m2K), double glazing window with argon chamber (U=2.0 W/m2K) or double glazing window with argon chamber high performance (U=1.0 W/m2K).

Once these three variables are selected by the user, the Web Server sends the request to the UBEM server to recalculate the demand values and updates the database, consequently displaying the map with the new data. When the recalculation is performed in the “building” visual mode, additional options become available (**Fig. 4** bottom left panel):

- EN 52016 simple model / detailed model. This option switches between the monthly calculation method and the hourly calculation method of the EN 52016.
- Passive mode /active mode. This option activates or deactivates the thermostat. When the passive mode is selected the building performs under free floating conditions. Consequently, the device will display the free-running indoor temperature. Upon selection of the active mode, a new option becomes available, enabling the modification of thermostat set points for cooling and heating.

2.4 Energy Model

2.4.1 Back-End. Energy model structure

The energy model has been adapted to the EN 52016-1:2017, the technical standard developed under CEN Mandate M/480 (Van Dijk & Hogeling, 2019) that supersedes the previous EN 13790:2008 (ISO, 2008). The EN 52016-1 specifies calculation methods for the assessment of internal temperature, sensible heating and cooling loads, based on hourly and monthly calculations (ISO, 2017b). The hourly calculation method takes into

account the dynamic interactions of weather, building operation, heat storage and solar radiation. It is a revised and more advanced version of the simpler method given in EN 13790:2008. The main difference is that building elements are kept separate in the new model, instead of being aggregated to a few lumped parameters as in the former (Van Dijk et al., 2016). Internal Mean Radiant, Air and Operative Temperatures can be obtained based on the hourly method.

The standard's approach is based on the thermal-electrical analogy. The heat flows are represented as a RC (Resistor-Capacitor) network, which describes the thermal resistances and thermal capacitances of both zones and buildings elements. The mathematical description consists of a discrete-time linear state space model, in which the states are the nodes' temperatures at the given time interval (x in eq. 1), the inputs are the boundary conditions (outdoor and ground temperature, solar radiation, internal gains, …) and the parameters are the energy flows defined by the thermal properties of the buildings. The resultant set of first-order differential equations can be solved by standard mathematical techniques with the assistance of programming libraries (e.g. NumPy).

$$\frac{dx}{dt} = A \cdot x(t) + B \cdot u(t) \qquad (1)$$

Where x(t) are the states of the system (temperatures), and u(t) are the inputs respect with time. A and B are the parameters that describe the resistance and capacitance of the system.

The EN 50216-1 provides a series of formulae for the description of the energy balance of each thermal zone and building element. Each one of those is defined as a branch of a RC-Network. The opaque building elements are discretized into four virtual layers, irrespective of the actual components, which may be lumped to fit the four-layer assumption (**Fig. 6**). The four layers are separated by five nodes, which can be interpreted as sensors measuring the node's temperature. The nodes are interconnected by four

resistances and attached to five capacities. Additionally, an internal air node reflects the air temperature of the thermal zone, while an exterior node defines the outdoor temperature from climatic data. Windows are represented by only two nodes, separated by a resistance but without a capacitance as their areal heat capacity is assumed as negligible. All surface nodes are affected by surface heat transfer coefficients, radiative and convective, which are calculated in accordance with EN13789:2017 (ISO, 2017a). External nodes may be subjected to a process of warming through solar irradiance, and cooling through additional thermal radiation directed towards the sky. The internal nodes are subject to the influence of various factors, including the internal gains, the heating and cooling (if applicable) and the solar heat gain transmitted directly into the designated zone. Roof and floor elements are represented in a similar way as the walls, as a 5-node RC-Network. However, certain values, such as surface resistance, are adapted to their horizontal position. Similarly, if the floor is connected to the ground, the external node is not the outdoor air but the ground itself, with different thermal dynamics. The procedures for calculating all these inputs and parameters are outlined in EN 52016:1:2017 and the various modules of the EPB standards (ISO, 2017b).

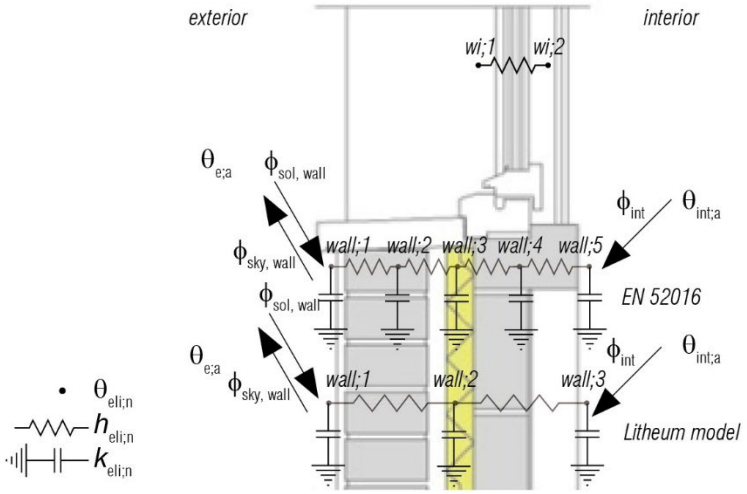

Fig. 6 Opaque wall and window element represented as RC-networks according to EN 52016:2017. The 3-node version assumed by Litheum model is shown at the bottom.

The Litheum model conceptualises each building in the study area as a single thermal zone as illustrated in **Fig. 7** and **Table 2**. For the sake of simplicity, the **Fig. 7** shows only the RC-network for one wall and one window. However, it must be noted that the model describes all external walls and their respective windows (if any) as separate RC-branches. The primary divergence from the EN 52016:2017 standard pertains to the utilisation of 3-node components for opaque elements, as opposed to the 5-node components employed in the standard. This assumption was based on three arguments: As demonstrated in previous research, the accuracy of lumped parameters at the element level (i.e. wall, roof or floor) is acceptable (Lundström et al., 2019; Ramallo-González et al., 2013). In the scope of this research, the temperature values inside the wall are irrelevant. The addition of further nodes per element has been shown to result in a substantial increase in the computational load, thereby compromising the application's lightweight nature. (Mazzarella et al., 2020).

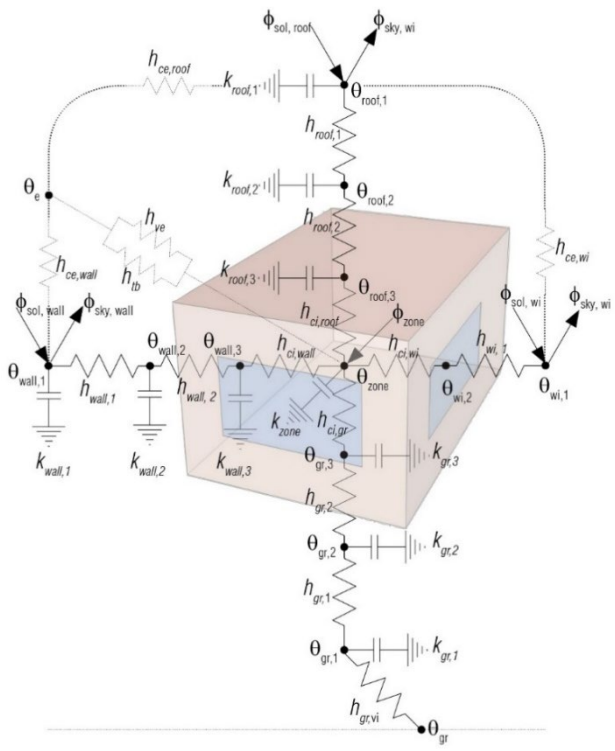

Fig. 7 *The RC-network representing the Litheum model*

Table 2 Main input parameters used for the Litheum model

Parameter	Description	Unit
Θeli,n	Node temperature, eli: element, n=node position (1:external, 2:inside, 3:internal)	ºC
Θzone	Indoor air temperature, zone	ºC
Θe	External dry bulb temperature	ºC
Θgr	Virtual ground temperature	ºC
heli,n	Thermal conductance between node n and node n-1on element eli	W/(m²·K)
hci	Convective heat transfer coefficient internal surface	W/(m²·K)
hce	Convective heat transfer coefficient external surface	W/(m²·K)
hve	Heat flow due to ventilation	W/K
htb	Heat transfer coefficient for thermal bridges	W/K
Keli,n	Areal termal capacity, element, node	J/(m²·K)
ϕsol	Solar irradiance on the element	W/m²
ϕsky	Extra-thermal radiation to the sky,	W/m²
ϕzone	Total internal heat gain, zone	W

The coefficients and terms of those formulae are carried over to a Matrix (Matrix A) and a Vector (Vector B) respectively. The thermal model is thus represented as:

[Matrix A] × [Vector X] = [State vector B] (2)

where [Matrix A] is a square matrix holding known system coefficients, [Vector X] is the state vector carrying the node temperatures to be obtained, and [State vector B] is a vector holding known boundary conditions and node temperatures from the previous time step.

The solver then iterates over the resultant numerical scheme to approximate a meaningful solution. Since the initial node temperatures are unknown (with the exception of the outdoor air temperature) the EN 52017 establishes a 14-days initialization period, which is meant to be “long enough to make the influence of the temperatures of each node at the start of the calculation negligible when the actual calculation period starts” (ISO, 2017d).

The Litheum model employs the hourly calculation method to obtain internal air, mean radiant and operative temperature under free running conditions when specific buildings are selected for detailed analysis. However, in order to ensure computational efficiency, the monthly method is used to calculate the initial energy needs for heating and cooling. The monthly method is a simplified procedure defined by the EN 52016. The thermal balance of the zone is determined on a monthly basis. The dynamic effects are taken into account by introducing the gain utilisation factor for heating and the heat transfer utilisation factor for cooling (ISO, 2017c). These parameters are functions of the heat-balance ratio and the thermal inertia and they vary for each month and operation mode (heating and cooling). The workflow of this method is illustrated in *Fig. 8* and *Table 3*. The relevant building information is stored in a JSON file that contains the whole city. Each building is an object that stores the cadastral reference, the envelope attributes and geometry, including the obstruction ratio. Additional tables and parameters and stored and retrieved in a separate module. This encompasses the internal occupancy patterns and associated internal gains, as well as the thermostat settings for heating and cooling. The meteorological data has been from the PVGIS database (EU Science Hub, 2024), which provides ready-to-use vertical and horizontal solar radiation data. The Litheum code extracts the heat gains and losses for each building and month as described by the monthly method. Subsequently, an analysis of the heat balance ratio for the heating and cooling modes is conducted. The energy loads to attain the desired indoor comfort temperature are calculated when additional heating or cooling is required.

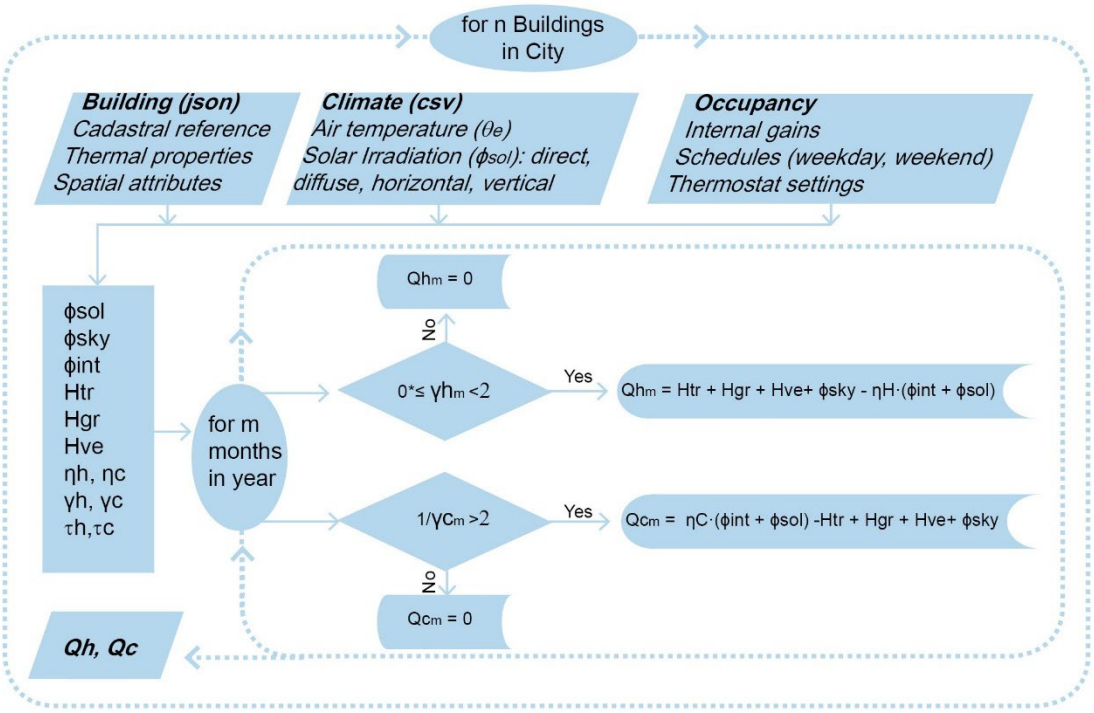

Fig. 8 Flow chart illustrating a simplified diagram of the code to calculate thermal and cooling energy needs using the monthly calculation method.

Table 3 Main parameters for the monthly calculation method

Parameter	Description	Unit
Qh	Total energy need for heating	kWh
Qc	Total energy need for cooling	kWh
Htr	Total heat transfer for thermal bridges	kWh
Hgr	Total ground heat transfer	kWh
Hve	Total heat transfer by ventilation	kWh
τh, τc	Time constant for the heating (h) and cooling (c) modes	h
γh, γc	Heat balance ratio for the heating (h) and cooling (c) modes	dimensionless
ηh, ηc	Utilization factor for the heating (h) and cooling (c) modes	dimensionless
ϕsol	Total solar heat gains	kWh
ϕsky	Extra-thermal radiation to the sky,	kWh
ϕint	Total internal heat gains	kWh

2.4.2 Urban data pre-processing

One of the primary objectives of the Litheum project is to consider the impact of the urban context on the energy demands of buildings. Consequently, the model considers the most relevant spatial characteristics of the built environment, such as solar obstruction, compactness, and orientation. In order to ensure replicability, the pre-processing steps of the spatial data were automated. Building-level pre-processing algorithms were developed and coded in Python to obtain individual buildings' exposed envelope area, as well as the solar obstruction in each orientation.

To calculate the exposed envelope, the code iterates over every floor of each building according to the following sequence: first, all buildings are sliced in the "n^{th}" using the cadastral vector layer. Then, the geoprocessing tool "buffer" is used to create parallel lines outwards and inwards to the sliced polygons. The code discriminates between exposed segments and internal partitions by analysing whether the outward buffer lines overlap the inner lines of any adjacent building. The lines that are part of the external envelope are classified as exposed and assigned an orientation based on their azimuth (**Fig. 9**). The orientations are classified into four quadrants (North, South, East and West). The calculation of the area of exposed envelop in each orientation, building and floor is achieved by multiplying the length of exposed segments by the floor height. This process is then repeated for each storey of the building, from the ground floor to the uppermost floor of the tallest building in the city. In conclusion, the table of attributes belonging to the building layer has been restructured in order to incorporate the total of the exposed envelop in all floors for each orientation. Consequently, four new fields were created and stored in the vector layer. These fields are labelled "Env_N", "Env_S", "Env_W", "Env_E", and they contain the area, measured in square metres, of the exposed envelope for each feature (i.e. building) in each orientation. These data will be used by the energy model to calculate the heat losses through the envelop as well as the heat solar gains. The

model will take into account the window-to-wall ratio, their respective orientation, and the obstruction angle accordingly.

Fig. 9 Exposed segments by orientation quadrants as part of the calculation process of the exposed envelope

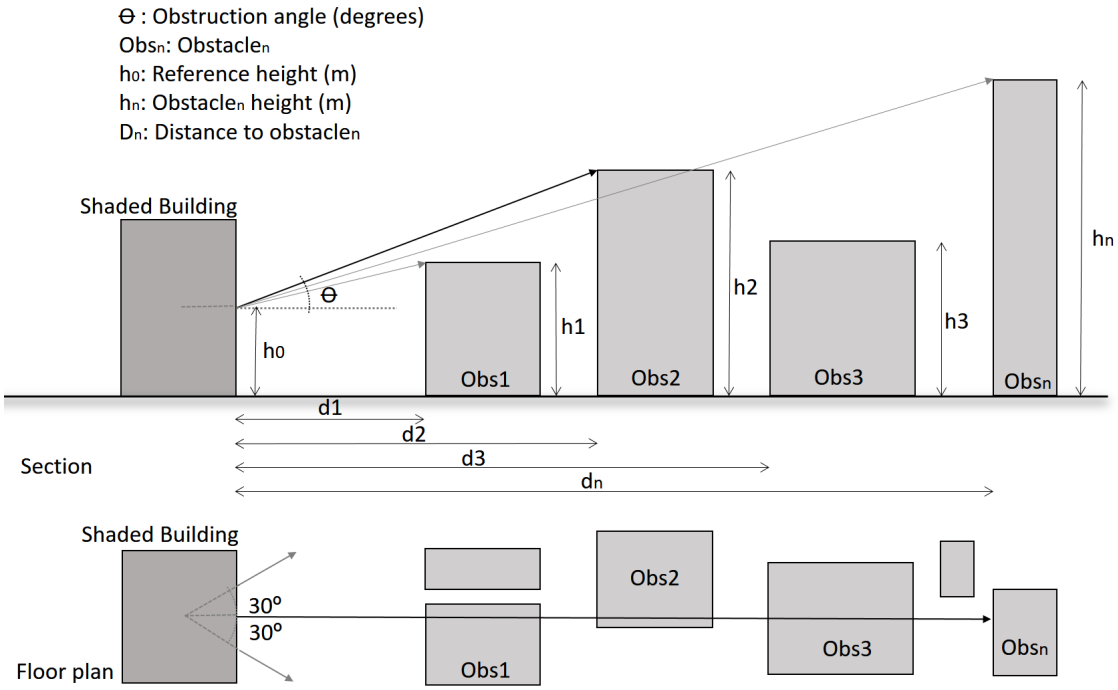

Fig. 10 Calculation procedure to obtain the obstruction angle for each orientation

In order to obtain solar obstruction, a Python module was created in PyQGIS (Dobias, 2023) to adapt the methodology regarding external obstacles as defined in the EN 52016-1 (ISO, 2017b p.187). This method involves the division of the skyline, as seen from the shaded façade, into four segments by three axes at 45-degree intervals. The obstruction

angle is determined for each individual axis, and then extrapolated for the interval under consideration. In the Litheum model, the façades were grouped in four main orientations, following the criteria described regarding the building envelope. For each orientation, the skyline was divided into six segments by axes at 30-degree intervals. However, since incident solar energy is known to decrease as the angle of incidence increases with respect to the normal, the axes at 60° and 90° from the normal were disregarded during the calculation of each orientation. The obstruction angle was calculated and averaged for the remaining three axes (normal and ±30 degrees). To this end, the code commences by tracing 12 axes at 30-degree intervals from the centre of each building. The axes intersect the building envelop polygon, as well as that of the surrounding buildings. The intersection points define segments that provide the distance between the analysed building and its obstacles on each axis. For each axis, the obstruction angle is calculated as the maximum obstruction angle created by all buildings intersecting the axis. The aforementioned angles are derived by calculating the arctangent of the obstacle's height minus the reference height (h_n and h_0 in **Fig. 10**) multiplied by the distance between the shaded building and the obstacle (d_n in **Fig. 10**). The process is then repeated for the four orientations and all buildings in the study area. It was determined that, given the code's high computing intensity, a maximum limit of 200m should be established for the length of the axes. The obstruction angle for each building, as well as its orientation, is saved and stored in the building vector layer. The obstruction angle for each building and orientation is saved and stored in the building vector layer, creating four new fields in the table of attributes: “Obs_N”, “Obs_S”, “Obs_E”, “Obs_W”.

3. Results

3.1 Litheum pilot cities

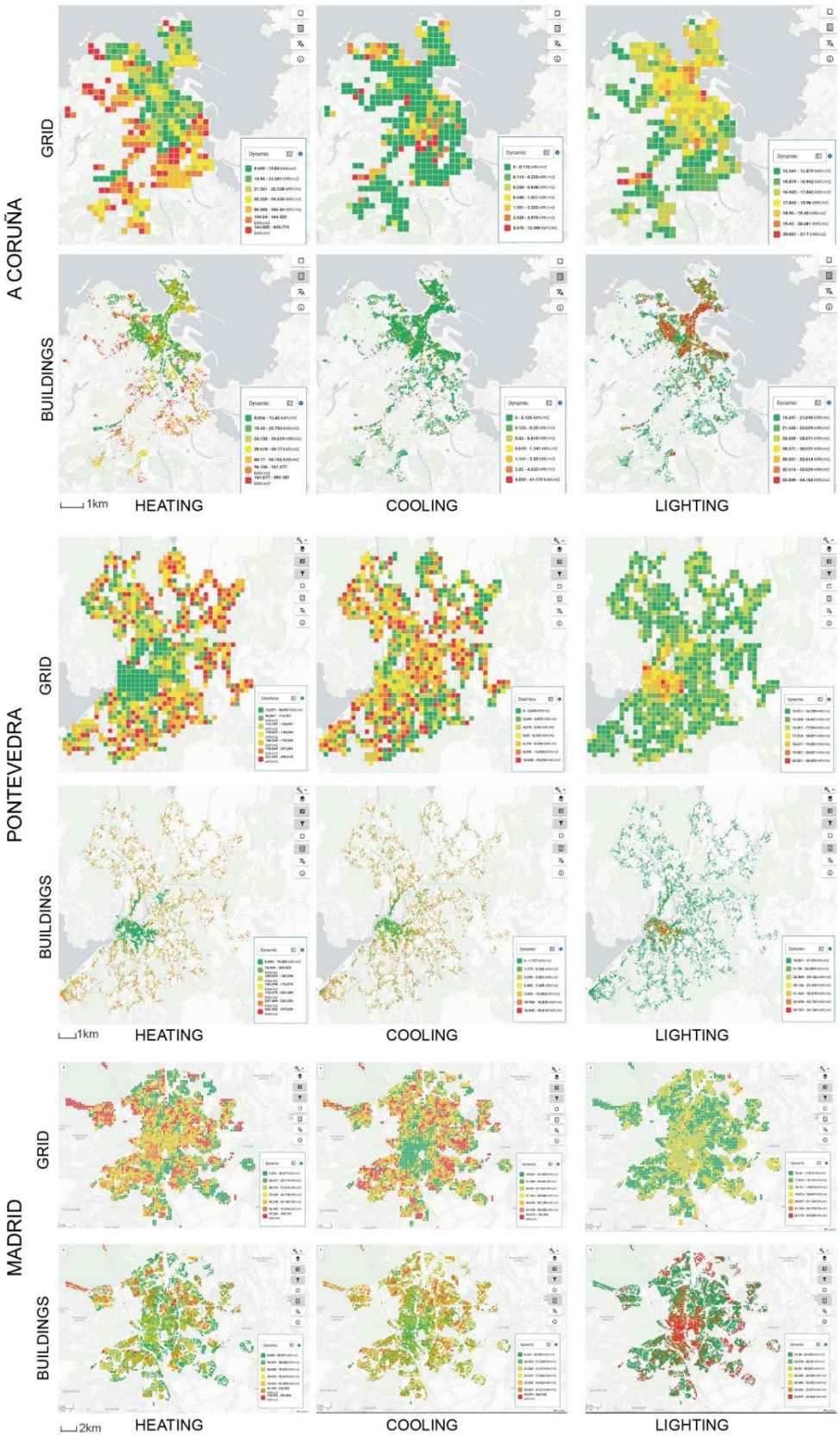

Fig. 11 Energy demand for heating, cooling and lighting demand for the three pilot cities. In each case the top row displays the results as a grid composed on 250x250m cells, the bottom row shows the results for each individual building, with a substantially finer resolution.

After setting up and testing the platform with a few urban samples, the next step was to develop pilot cases in selected cities. The approach was to start with a small municipality to detect and handle possible glitches. Issues detected in the first pilot could be prevented in subsequent ones, which would gradually increase in size. The first pilot city was Pontevedra, a mid-size municipality of 83,000 inhabitants in northwest Spain. It had approximately 10,000 buildings, many of which were detached housing. This city was selected due to ongoing collaboration between the research team and the city council, enabling continuous feedback and interaction. The second pilot city was A Coruña, 120 km north of Pontevedra, with a population of 240,000 inhabitants. It has slightly over 18,000 buildings due to its density and compact nature. As in the previous case, easy access to planning authorities was key to selecting this city as the second pilot. The third case study was Madrid, the fourth biggest city in Europe with a population of 3.2 million residing in over 125,000 buildings. Its urban structure is characterised by dense housing blocks in the central areas and suburban satellite towns on the periphery. Unlike the previous two cases, the main reason to select Madrid as the third pilot was to test the preparation methods and functionalities of the platform on a large scale. It also provides a continental climate, which differs substantially from the other pilots. It was expected to present higher heating and cooling loads due to larger seasonal variations. **Fig. 11** shows the results for the base layer in the three pilot cases, displayed as a grid and per building. The maps suggest a correlation between high density and relatively lower heating load. This corresponds to the city centres of Pontevedra and Coruña, while in Madrid the heating performance is more evenly distributed. Overall, the cooling demand in the northern cities is low. In Madrid, overheating seems a critical issue, with values starting from 20 kWh/m² and reaching up to 50 kWh/m². It must be noted that neither solar control nor the heat island effect were introduced in the base layer. Solar control has been modelled as an energy conservation measure that can be selected by the user. The heat

island effect can be introduced in the pre-processing steps and is expected to be included in future model developments. The lighting demand maps follow the logic of dense areas presenting a lower sky view ratio from windows and, consequently, less daylight and higher dependence on artificial lighting.

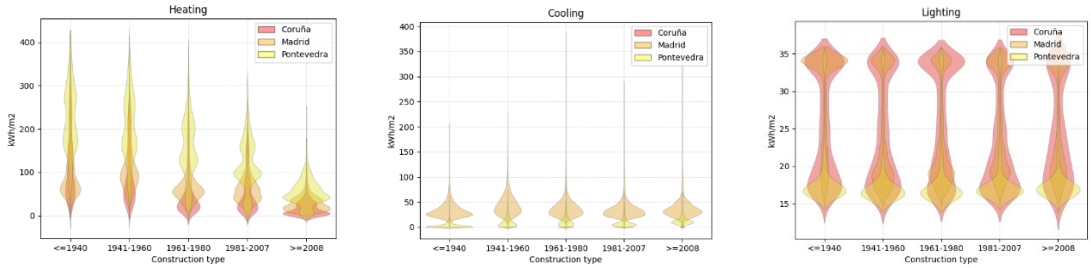

Fig. 12 Distribution of annual energy demand at building level in the three pilot cities. The graphs show the relation between construction types and heating, cooling and lighting loads in the three cases.

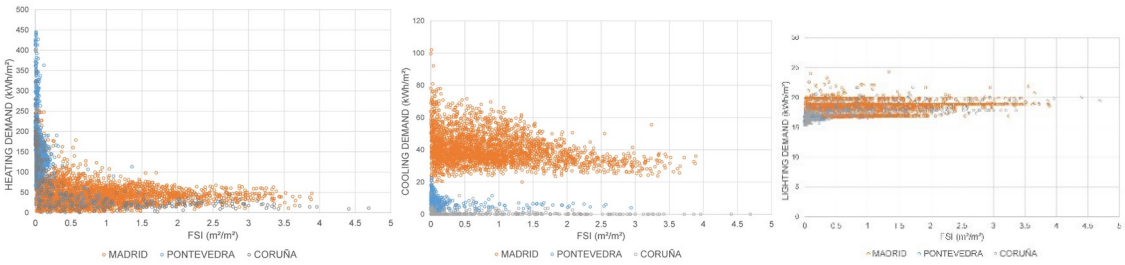

Fig. 13 Graph illustrating energy demand as a function of FSI, data obtained from the grid layer.

The pilot study results were analysed further to reveal inconsistencies across cities, climates and typologies. *Fig. 12* shows the relation between construction types and heating, cooling and lighting loads in the three cities. It is based on the individual building base layer. Heating load is lower in newer buildings, as expected. Older buildings have a higher result dispersion, suggesting variations in the form of poorly insulated buildings. Pontevedra has the highest heating load, due to abundance of single family housing. Madrid and Coruña have mostly flats, which have a lower exposure and therefore suffer less heat loss. Coruña has negligible cooling loads and Pontevedra relatively low cooling loads. Madrid has similar lighting loads across types, although they tend to be slightly

higher in newer buildings and lower in the oldest. The lighting loads in the three cities follow similar distributions, with a concentration of observations between 15-20 kWh/m² and a second cluster around 33 kWh/m². These values are in accordance with the region's domestic lighting energy consumption benchmarks, which are 26 kWh/m² (Cadima & Rodríguez Álvarez, 2021). The highest value could be due to artificial lighting and the lowest value to passive potential. Pontevedra's buildings have the largest daylight potential, probably due to their lower density and greater sky view ratio.

The previous observations were compared against a parametric analysis relating urban density and energy demand (**Fig. 13**). In this instance, the results are grouped according to the grid layer as opposed to individual buildings. Each dot in the scatter plots represents one grid cell's average demand. Density is measured as Floor Space Index (FSI), a common metric in urban planning relating total built-up area per unit of land. Results are consistent with previous graphs, though there's a smoothing effect due to the use of average values. This is particularly noticeable in lighting loads, where demand is clustered around 20kWh/m². Graphs show morphological variations across cities. Pontevedra has a larger proportion of cells with a FSI below 0.5m²/m², indicating low density. Madrid and Coruña show higher values of up to 3.5m²/m². Overall, low density is associated with higher heating and lower lighting demand. The characteristic building typology in these areas is detached housing, which is known to be more thermally inefficient than flats in temperate climates. Cooling load diminishes with high density due to overshadowing. However, density can also enhance the heat island and reduce ventilation potential (e.g. due to obstruction, pollution or noise), factors not introduced in the model.

3.2 Validation and verification

The model's methodology and assumptions underwent validation in accordance with the verification procedure of the EN 52016, a process that draws inspiration from the ANSI/ASHRAE standard 140 (ANSI/ASHRAE, 2014). The test case, entitled Bestest, provides a comprehensive overview of the primary inputs, including geometry, thermophysical properties, boundary conditions, and climatic data. It also presents the subsequent results for a range of scenarios, namely lightweight construction (designated as 600) and heavyweight construction (designated as 900). These scenarios are examined in conjunction with continuous and intermittent heating, as well as free-running conditions, which serve as control strategies.

Recent studies have revealed discrepancies between the EN 52016 and detailed thermodynamic models (De Luca et al., 2022; Zakula et al., 2021). In order to establish a more comprehensive comparative framework, the Bestest model was also simulated in EnergyPlus v.24.2.0 using the OpenStudio platform v.3.9.0 (NREL et al., 2023). The energy demand estimates obtained from the Litheum model were then compared against those provided by the EN 52016 (EN) and EnergyPlus (E+). models The outcomes obtained in the verification process provide empirical evidence that validates the Litheum model for large-scale urban analysis.

For the purposes of this validation, the Litheum model was adapted to the Bestest specifications; this refers to a geometry consisting of a single zone with an area of 48m² and a height of 2.7m (*Fig. 14*). All constructions are regarded as external, with no consideration given to shading or obstruction by adjacent buildings. The EN 52016 model utilises an oversized floor insulation layer with the objective of decoupling the slab from the ground, thereby reducing potential uncertainty regarding the thermal dynamics of the ground. Consequently, the verification methodology indicates that the ground node can be assumed as another outdoor node, with outdoor air temperature as the boundary

condition (ISO, 2017c p.123). The standard specifies the attributes of the opaque elements in detail, for each layer and element, and as a compound, for hourly and monthly calculations respectively. The main thermal properties are summarized in *Table 4*.

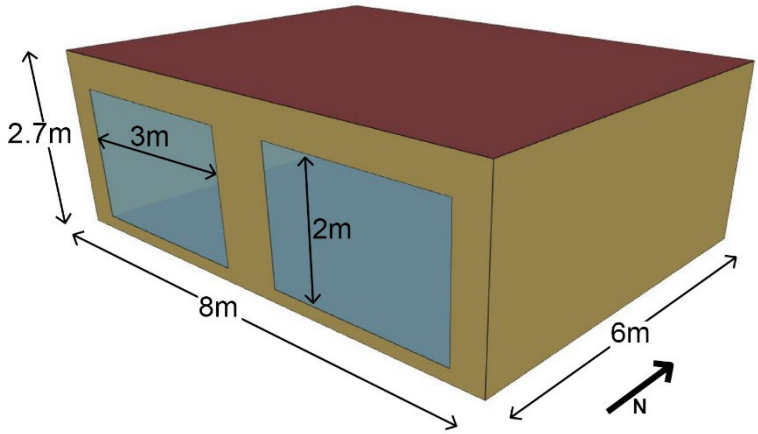

Fig. 14 Geometry of the test room (bestest) as modelled for validation in Litheum, EnergyPlus and EN 52016

Table 4 Thermal properties of the test case

U-value (W/m²K)				Solar Transmittance (glazing)	Infiltration (AC/H)	Internal Heat Gains (W)	Thermostat (ºC)		Heat (MJ/K)		Capacity
Wall	Roof	Floor	Window				Heat	Cooling	Light	Heavy	Air & furniture
0.56	0.33	0.04	2.98	0.71	0.41	200	20	27	3.84	12.48	0.48

The climatic data used is the Drycold Typical Meteorological Year, which is based on values from Denver, Colorado (United States). It can be found at the ISO website (ISO, 2016) or at the NREL Energy Plus repository in epw format (NREL, 2014).

The results of the verification cases are provided for both the monthly method and the hourly method. With regard to the former, the comparison is drawn for the annual sensible energy needs for heating and cooling. The EN 52016 assumes that the monthly method is calibrated for each region using coefficients derived from the hourly method (Van Dijk

et al., 2015). Regarding the hourly calculation, the analysis incorporates monthly average values for the operative temperature, and the hourly breakdown of sensible energy needs for heating and cooling, as well as the operative temperature for January 4th and July 27th (ISO, 2017c p.130). The standard provides a series of tables with the results for each scenario and calculation methodology. The verification tests are conducted by calculating the operative temperature and energy loads using the Bestest specifications in Litheum and E+. The results are compared against the standard's tables.

The initial series of simulations was done using the monthly method. The EN standard cautions that given the method's reliance on numerous optional coefficients contingent on particular regional circumstances, reliance on a single test case for verification is impractical (ISO, 2017b p.122). Therefore, the monthly method has been also compared against EnergyPlus in order to calibrate and verify the Litheum algorithm The results shown in *Table 5* suggest that there is a good approximation to the EN model for the heating demand in both the lightweight and the heavyweight cases, and for cooling in the lightweight case, with a deviation below 12% in all cases. However, the cooling estimate of the Litheum model for the heavyweight scenario diverges from the EN model while it is very close to the EnergyPlus, with a variation of less than 5%. Subsequent to conducting further tests to ascertain the origin of the discrepancy, it was determined that the cause could only be attributed to the application of differing calibration coefficients.

Table 5 Results for annual heating and cooling demand using the monthly method

	Bestest600			**Bestest900**		
	Litheum	**EN**	**E+**	**Litheum**	**EN**	**E+**
Heating (kWh)	5511	5133	3498	2967	3360	2908
Cooling (kWh)	6875	7503	6698	2689	76	3776

The second run of simulations focused on the calibration and verification of the hourly method. The generation of the test cases was based on two thermal capacities, designated lightweight (600) and heavyweight (900), and two operational modes, designated AC for active mode and FF for free floating. These scenarios were then subjected to evaluation using three models (Litheum, EN and E+) for a total of 12 comparative cases. As illustrated in *Table 6* the average operative temperature is presented for each case, calculated on a monthly basis. A close correspondence across the board can be observed. A more detailed analysis reveals a certain disparity in the heavyweight free-floating conditions. The results obtained from the EnergyPlus model consistently demonstrate higher values in comparison to those derived from both the Litheum and EN models. The divergence is more pronounced in winter than in summer, and this is attributed to the different physical assumptions and formulations used in EnergyPlus (U.S. Department of Energy, 2024). Nevertheless, the Litheum and EN models demonstrate a high degree of similarity, with a maximum disparity of less than 2 degrees Celsius, consistently maintaining a margin of 1 degree.

Table 6 Test results average operative temperature

	Avg Operative Temperature (ºC)											
	600AC			**900AC**			**600FF**			**900FF**		
Month:	**Litheum**	**EN 52016**	**E+***	**Litheum**	**EN 52016**	**E+***	**Litheum**	**EN 52016**	**E+**	**Litheum**	**EN 52016**	**E+**
JAN	22.1	22.0	21.8	22.1	22.3	22.9	17.0	17,3	18.0	17.2	17,6	21.6
FEB	22.2	22.0	21.8	22.1	22.2	22.7	16.9	16,7	17.7	16.4	16,4	20.5
MAR	22.7	22.6	22.7	22.9	23.1	24.1	21.8	22,1	22.7	21.6	21,9	25.5
APR	23.0	22.9	23.1	23.7	23.9	24.8	24.0	24,3	24.9	24.4	24,7	27.4
MAY	23.6	23.5	24.0	24.6	24.5	25.8	26.6	26,7	27.4	26.4	26,6	28.8
JUN	24.2	24.4	24.9	25.6	25.7	26.8	29.2	29,6	30.2	28.8	29,3	31.2
JUL	25.1	25.6	26.4	26.6	26,6	27.9	34.1	35,0	35.3	34.0	34,9	36.7
AUG	24.6	25.2	26.0	26.5	26,6	28.0	34.6	35,2	35.6	34.6	35,2	37.3
SEP	23.9	24.2	25.1	25.8	26,1	27.7	33.6	34,6	34.9	33.8	34,7	37.6

OCT	23.0	23.0	23.7	24.3	24,8	26.3	28.5	29,7	29.7	29.2	30,3	33.6
NOV	22.3	22.2	22.3	22.5	22,8	23.8	21.1	21,4	22.1	20.9	21,3	25.3
DEC	22.1	22.1	21.9	22.1	22,2	22.9	17.4	17,9	18.5	17.6	18,0	22.2
Annual Avg.	23.2	23.3	23.7	24.1	24.2	25.3	25.5	25.9	26.5	25.5	25.9	29.0

The annual results are displayed in Table 7, which denotes a coherent performance of the three models. The main discrepancies, which are found in the active mode operative temperatures, are clearly associated with the thermostat controls, which are based on Operative Temperature in the EN standard and, consequently in Litheum as well, while they are based on air temperature in EnergyPlus. The thermostat setpoint was set at 20°C and 27°C for heating and cooling, respectively. Consequently, the resulting values are an exact reflection of these settings, with the exception of EnergyPlus, in which the air-based control allows for higher and lower operative temperature values. However, these discrepancies are substantially minimized in the free-floating conditions. Notwithstanding the inclusion of the most extreme scenarios in the EN standard, it is evident that such events are improbable in reality due to behavioural adaptation. Consequently, the variations are negligible and can be considered to fall within a reasonable margin of error.

Table 7 Test results annual hourly integrated peak heating and cooling, loads, maximum, minimum and average operative temperature

	600AC			**900AC**			**600FF**			**900FF**		
	Litheum	EN 52016	E+*	Litheum	EN 52016	E+*	Litheum	EN 52016	E+	Litheum	EN 52016	E+
Heating	4,227	4,351	3,498	3,855	4,067	2,908	--	--	--	--	--	--
Cooling	6,180	6,363	6.698	3,738	4,043	3,776	--	--	--	--	--	--
Max. Op Temp	27.0	27.0	33.4	27.0	27.0	31.5	65.4	63.5	63.5	43.6	44.4	48.5

Min. Op. Temp	20.0	20.0	16.1	20.0	20.0	16.7	-19.7	-16.9	-16.0	-2.0	-2.4	-0.2
Average	23.2	23.3	23.7	24.1	25.9	29.0	25.5	25.9	26.5	25.5	26.0	29.0

The monthly breakdown of the heating and cooling loads confirms the earlier observations as illustrated in *Fig. 15*. The Litheum model and EN 52016 are consistently aligned while the EnergyPlus results are slightly underestimated. However, as it was explained above, the different thermostat control explains this variation. Moreover, it can be noted that the relative values are consistent. The demand for cooling and heating energy rises and drops following the same patterns in the three models. The subsequent test focused on the hourly performance of the models. This analysis illustrates the potential of dynamic models as they reflect how the building fabric is influenced by its thermal capacity. The study took the 4th of January as a representative day. Although it is a very cold day the internal temperature and energy loads fluctuate quite dramatically over the 24 hours due to the settings proposed in the Bestest by the EN 52016 standard. It provides a sound base to compare the model predictions. *Fig. 16* shows the hourly energy load for the Lightweight and the Heavyweight tests. Despite outdoor temperature being consistently below zero, the south elevation has strong vertical solar radiation, reaching nearly 1000W/m² at noon. Consequently, there is a need for cooling in the Lightweight case during the central hours of the day. By contrast, the Heavyweight case shows the effect of thermal mass to mitigate the solar gains and completely remove the cooling load. This pattern in repeated across the three models, with only the EnergyPlus result reflecting, again, the effect of its different thermostat settings, based on air rather than operative temperature. Finally, *Fig. 17* portrays the closest similarities among the models' predictions. In the Lightweight case, the Litheum model slighlty underestimates the minimum temperature, but matches the EnergyPlus results between 9am and 4pm, and

the EN 52016 from 4pm to 8pm. In the Heavyweight case, the three models show the same temperature during the night, but differ slightly during the day. The Litheum results are in between the EN 52016 (2-3K below) and the EnergyPlus (2-3K above).

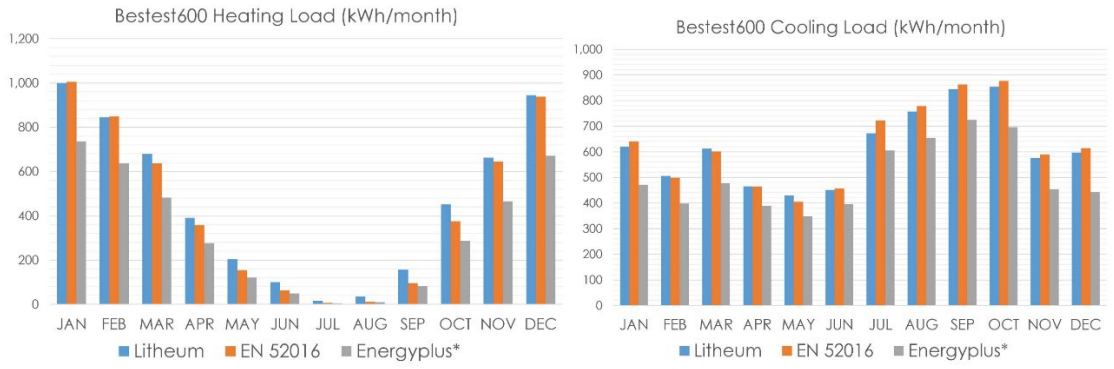

Fig. 15 Test results of the hourly method. Hourly values for Heating (left) and Cooling (right) loads for the Lightweight case

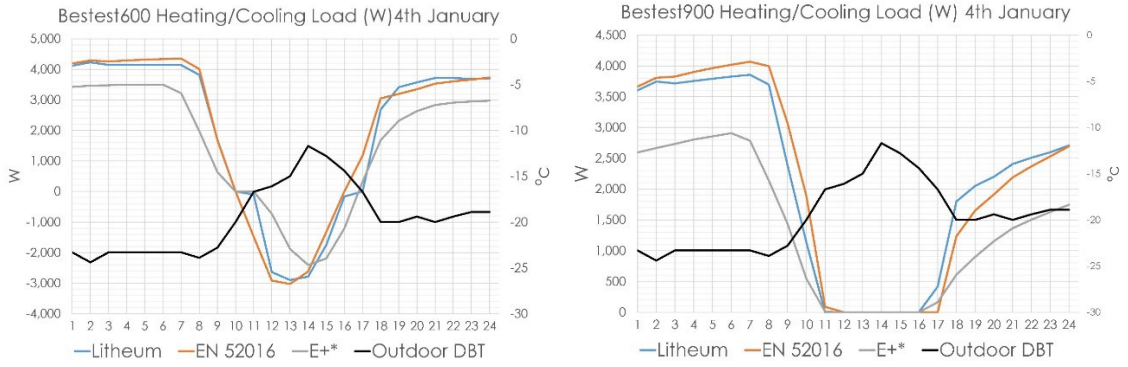

Fig. 16 Test results of the hourly method. Hourly values for Heating (positive values) and Cooling (negative values) loads the 4th of January, for the Lightweight case (left) and Heavyweight case (right)

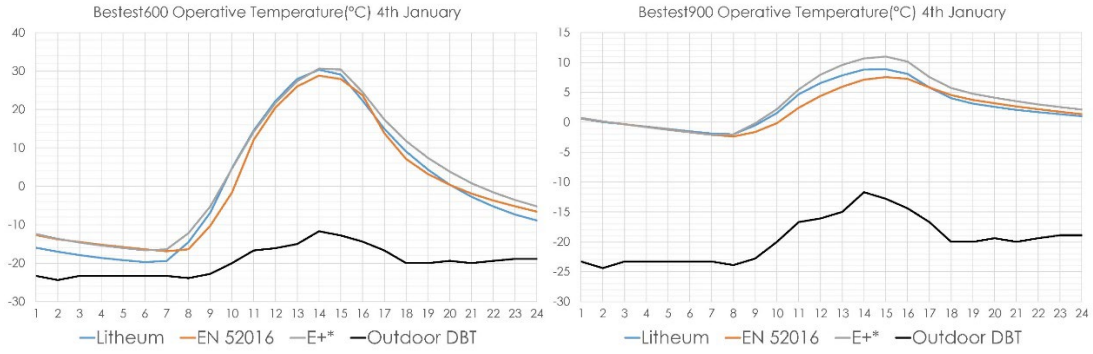

Fig. 17 Test results of the hourly method. Hourly values for Operative Temperature on the 4th of January, for the Lightweight case (left) and Heavyweight case (right)

4. Discussion

This paper introduces a new approach for analysing the influence of urban morphology on the thermal and lighting performance of domestic environments. The context of a building's surrounding urban fabric affects solar access and the exposure of the building's envelope. This may occlude the path of direct solar radiation, which is the main natural heating gain. Neglecting this may lead to overestimating the heating demand (Ratti et al., 2005). The model accounts for solar obstruction at each building, using monthly and hourly methods. It also considers the proportion of the external envelope to floor area, as this affects conductive heat flow. The model computes all external elevations that are directly exposed to the outdoor environment. Buildings with party walls have different boundary conditions than detached constructions, usually resulting in reduced heat flow. The model calculates the proportion of shared walls and assumes equal conditions in both buildings, thus removing any heat flow across the shared element.

As explained in section 2.4.1, the model diverges from EN 52016 by dividing opaque building elements into three nodes instead of five. The standard (ISO, 2017c p.68) explicitly allows alternative options for the subdivision of each construction element. Furthermore, the method outlined in the previous standard EN 13790 (ISO, 2008), is based on three nodes and a first order system (5R1C), where all building elements lumped into a single capacitance. This simplified version has been used in various recent UBEMs (see for instance, Fonseca & Schlueter, 2015; Kastner & Dogan, 2024; Kristensen et al., 2018; Zarrella et al., 2020). The assumptions of the Litheum model are fully aligned with the parameters of the EN 52016. Despite the reduction in nodes each opaque building element (floor, walls and roof) is modelled separately, and thermal mass is distrusted in

two layers (internal and external). This retains the main advantages of the updated modelling method. Heat flows can be connected to their specific environmental conditions, taking into account the differences in temperature and radiation on roof, wall, and ground elements. The thermal mass can be specified for each element, taking into account its position, which influences the surface temperature and subsequently the zone's mean radiant temperature.

Second-order RC methods such as Litheum are currently widely used for modelling building heat transfer (see for instance, Bueno et al., 2012; Fabre et al., 2018; Harish & Kumar, 2016; Wang & Xu, 2006). A review of the literature reveals a growing consensus that second-order models are highly accurate and that increasing complexity does not significantly improve performance (Harb et al., 2016; Z. Wang et al., 2019; Yang et al., 2024).

In the context of city-wide building energy simulations, the complexity and heterogeneity of the building fabric render detailed physical modelling computationally impractical. While thermodynamic methods such as the conduction transfer function, as implemented in EnergyPlu (U.S. Department of Energy, 2024), are accurate at the building level, they have limited scalability for large urban applications. In contrast, RC networks enable the efficient simulation of large building stocks, thereby facilitating comprehensive urban energy assessments at city scale.

Detailed thermodynamic simulation tools use shadowing algorithms to compute sunlit areas at each time step. Rendering tools intended for image visualization have developed sophisticated ray-tracing techniques, whereby light reflected by an object is projected backwards from the target plane to the source(s) (Andersen & De Boer, 2006; McNeil et al., 2013). However, thermal applications do not require such accuracy; instead, they rely on simplified radiation exchange models (Robinson, 2011). For instance, Energyplus

is based on solar geometry and classic studies. The solar position is described in terms of three direction cosines (U.S. Department of Energy, 2024). Building and obstructions are then described geometrically using a coordinate transformation, from world to relative coordinates (Groth & Lokmanhekim, 1969) and, finally, the shadow projection is determined after Walton's algorithm (Walton, 1978). This approach has certain limitations regarding non-convex geometries, which are not considered. An alternative approach is the Sky View Factor (SVF), which models obstructions to the sky from a point or surface (usually represented by its central point) over the course of the year. Hourly solar radiation can thus be estimated by overlapping the SVF with the Sky Radiation Model (SRM) (Marsh, 2004; Teller & Azar, 2001). These methods are intended for individual buildings or small developments, and they are impractical for large scale models. Therefore, the Urban Building Energy Model (UBEM) needs to make certain assumptions in order to be manageable. Baker and Steemers proposed the Urban Horizontal Angle (UHA) as an average obstruction in the field of view of the analysed elevation(Baker & Steemers, 2000). Pili et al (Pili et al., 2018) analysed the accuracy of the discretization of the visible skyline for various subdivision angles using Digital Elevation Models. Litheum adapts this approach to external obstacles as defined in the EN 52016 (ISO, 2017b p.187). The skyline is divided into eight segments, with four segments always in view of the shaded façade, as described in Section 2.4.2. Despite the assumptions and simplifications, calculating the obstruction angle remains time-consuming for large cities.

It was observed that the execution of the code slowed down exponentially as the number of buildings in the analysed sample increased. For example, processing a sample of 277 buildings took 26 seconds, equivalent to 0.1 seconds per building. However, applying the same algorithm to a sample of 1,600 buildings took 11 hours, resulting in 25 seconds per

building. For a sample of 5,000 buildings, the average processing time was 60 seconds per building. Repetitive iteration over all buildings to determine the shading mask was identified as the cause of the delay. Subsequently, an optimised model divided the city into different zones of a similar size using the k-means clustering algorithm (Dobias, 2023). This reduced the processing speed by an order of magnitude. Madrid, with over 120,000 buildings, took nine days to process, equivalent to an average of six seconds per building. While it remains a computationally intensive task, it only needs to be performed once for each city. The values stored in the building database will not vary unless there are modifications to the urban fabric (e.g. new urban developments are added). Furthermore, piecemeal urban transformations can be introduced without the need to compute the entire city. Current work on this topic focuses on optimising this process using artificial intelligence techniques.

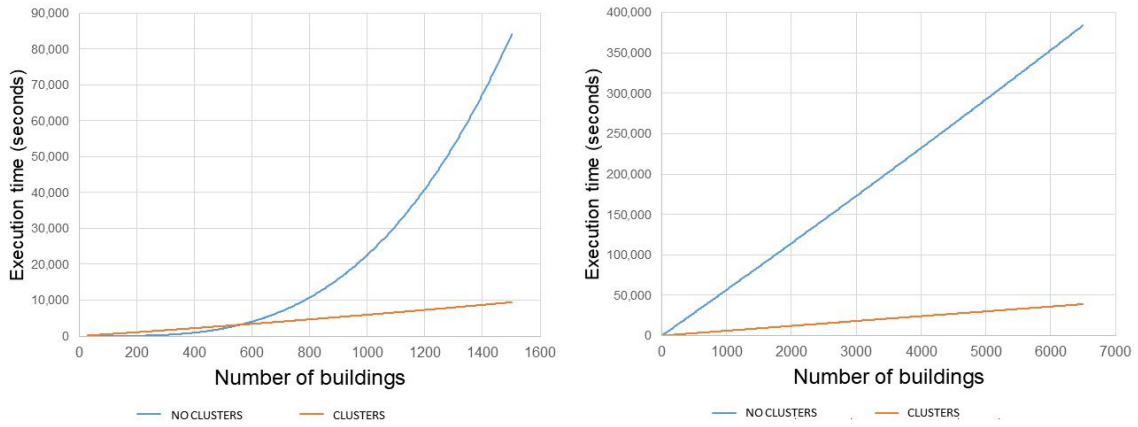

Fig. 18 Obstruction angle code execution time in relation to the number of buildings in the sample, without and with clustering. Left: The initial pattern shows nearly exponential increase in computing time. Right: the trend stabilizes as a linear increase beyond two thousand buildings. The python code was executed in a desktop PC, Intel Core I5, 6 cores, 32 GB RAM

Calculating exposed building envelopes is not nearly as computationally intensive as calculating obstruction angles. Previous studies used DEM to derive the area of the resultant surfaces, which by definition are all external in this specific format (Rodríguez-

Álvarez, 2014). However, as with the obstruction angle vector data was chosen due to its greater precision. Using the obstruction angle and building morphology as input parameters enables meaningful characterisation of the effect of the urban fabric on domestic energy consumption. However, energy maps based on typological statistics do not reflect the specificity of each building; they homogenise demand distribution because they only reflect a number of predefined typologies. Regardless of their level of detail, these typologies fall short of encompassing actual urban complexity. *Fig. 19* illustrates five linear blocks of similar characteristics, portrayed by Litheum (left) and an typological model without urban context (right). The latter assigns the same demand to all buildings because they have the same age and similar geometry. However, Litheum is more sensitive to buildings in corners, which have greater exposure, and to buildings with lower obstruction.

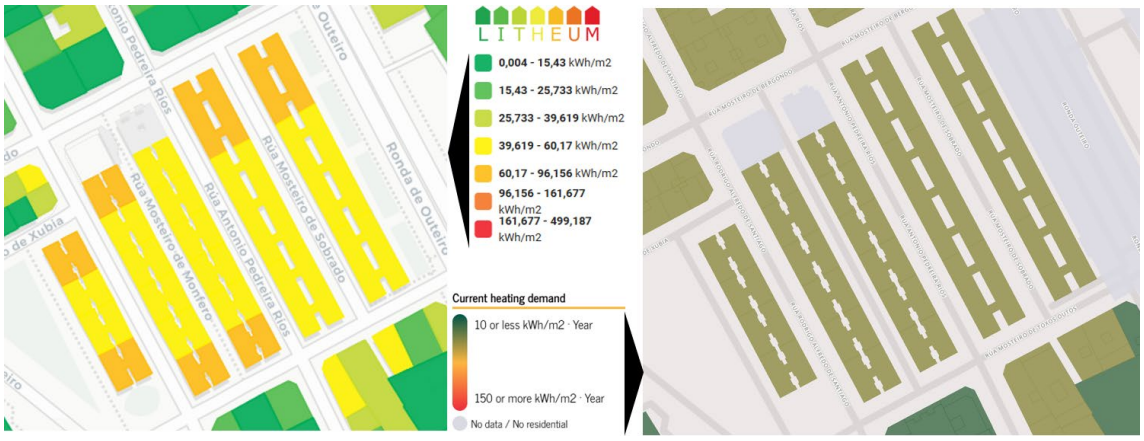

Fig. 19 The energy model in Litheum takes into account the obstruction angle and envelope exposure of each building, (left). The map on the right shows the same area as represented by the Urban3R project (Ciclica, 2023)

4.1 Uncertainty and potential improvements.

Like most UBEMs, the Litheum model is limited by the quality of the input data. The absence of a comprehensive database containing the thermal properties of buildings means that relevant parameters must be inferred from known attributes. This is a common

approach and, moreover, forms the basis of statistical models (Ciclica, 2023; Hallik et al., 2024). There is a strong relationship between age and thermal transmissivity; for instance, a recent study applied Artificial Neuronal Networks to predict the U-value of opaque elements with a correlation coefficient of 0.967 (Álvarez et al., 2018). In contrast, the window-to-wall ratio has a weak relationship with any known attribute, requiring complex techniques that typically involve image analysis (Szcześniak et al., 2022; Zhuo et al., 2023). Notably, the latest update of the Spanish Energy Performance Certificate (EPC) registry includes the window-to-wall ratio of certified buildings in its digital database (Villanueva-Díaz et al., 2024) and work is ongoing to derive accurate prediction models for the building stock. The modular nature of the Litheum structure enables these potential improvements to be integrated seamlessly.

The definition and priorities of UBEM depend greatly on the intended application and scale. Modelling techniques must be tailored to the specific objectives and scope of the analysis. RC models offer several advantages, including flexibility, adaptability, and fast computing times (Yang et al., 2024). However, this flexibility has also led to a wide array of different approaches, creating a heterogeneous theoretical ecosystem which has been described as confusing and lacking clear conventions (Y. Li et al., 2021). RC models have advanced progressively from analysing simple envelope elements to multi-zone buildings and urban scales. Applications include the estimation of building energy loads (Rouchier et al., 2018) , control and optimization at zone, building or grid level (Berthou et al., 2014), and micro-climate analysis (Bueno et al., 2012), among others. Modelling methods are commonly divided into three categories [a] white-box or forward models, [b] black-box, inverse or data-driven models and [c] hybrid or grey-box models, which are a combination of the previous two approaches. (Ali et al., 2021; Harish & Kumar, 2016). Forward models use known spatial and construction information (e.g. building form and

material properties) to simulate a building's environmental behaviour under predefined boundary conditions. Data-driven models are based on measured data, which are used to train and calibrate the models. Consequently, white-box models are suitable for estimating energy loads during the design and planning stages, when the thermal properties are known, but it is not possible or practical to conduct actual observations. Black-box models are widely used for system and grid control, fault detection, and performance optimisation in existing buildings, provided that observations and performance data are available (Z. Wang & Chen, 2019). In the absence of observations, data-driven models can be derived from simulated data thus creating hybrid models (X. Li & Yao, 2021; Seo et al., 2022). The development of Litheum was developed based on the energy calculation methods of the EN 52016, and the use of the state-space representation defined in the standard to solve the system. This method does not require actual measurements, and it is validated by comparing it with the Bestest model. The model provides energy load estimates based on specific climate, urban form and building characteristics. Behavioural patterns, socio-economic aspects, and system efficiency are given pre-defined values (as described in the methodology section), which can be considered generic. Differences between energy loads and actual energy consumption in measured data are expected due to the aforementioned factors. The Litheum approach favours transparent definition and evaluation of large-scale retrofit scenarios based on construction improvements (e.g. insulation or windows), excluding the effects of factors involving greater uncertainty, such as operation and efficiency.

The feedback interaction between buildings and the urban climate may induce significant variations in energy performance within a city (Sezer et al., 2023). Various studies have estimated that the impact of the Urban Heat Island effect on building energy loads is in the range of 10–20% (X. Li et al., 2019; Santamouris, 2014; Santamouris et al., 2015).

However, many building regulations and conventional energy modelling approaches rely on coarse climatic classifications (Walsh et al., 2017) and data from weather station data which do not consider microclimates (Huang et al., 2020). Consequently, the results from these models do not account for the specific local wind flow, air temperature or anthropogenic heat when defining boundary conditions across the city. Some applications do not require such level of accuracy as they prioritize relative performance trends. For example, comparative building retrofitting scenarios, where the goal is to identify the most efficient solutions rather than predicting the actual grid load. The Litheum model uses climatic data from PVGIS, which collects information at the mesoscale (EU Science Hub, 2024). Currently, the calculations assume the same outdoor boundary conditions for all buildings. However, future will involve integrating a detailed Urban Climate Model (UCM) to upgrade Litheum as a Multi-Domain Urban Scale Energy Modelling (MD-USEM). Previous experience and recent reviews in this area (Pasandi et al., 2024; Sezer et al., 2023; Sola et al., 2020) suggest that a tool such as the Urban Weather Generator (UWG) could incorporated into the model as an additional layer (Bueno et al., 2013). The UWG combines an urban canopy and building energy model based on an RC network to generate site-specific urban weather files (Bueno et al., 2012). These files could then be distributed evenly across the city to identify relevant microclimatic patterns and create an urban climatic model, replacing the current climatic module.

5. Conclusions

This paper presents a UBEM that integrates morphological sensitivity and the interactive definition of alternative scenarios. The model combines an innovative method of characterising urban form and building properties with calculation methods defined by EN 52016. Integrating the model into a user-friendly online platform makes it accessible

to a wide range of users, from homeowners to policymakers. The main insights from this research are as follows:

First, a surge in the development of UBEM tools has been observed in the last two decades. However, many of these projects have been discontinued or remain inaccessible due to commercial schemes, hyper-specific formats, and steep learning curves, which limit their potential uptake. Litheum was implemented using open-source solutions for its geographical features and relational database (GeoJSON and PostgreSQL, respectively), and it can easily be adapted to various spatial standards. The application is intuitive and targeted at regular users with no prior experience of energy modelling. The energy conservation measures have been predesigned and are limited to the most common retrofitting solutions, striking a balance between flexibility and simplicity.

Data-driven energy models are less sensitive to parameters related to the urban context, such as overshadowing caused by adjacent buildings. They rely on typological statistics that connect known parameters, such as age, to energy performance. In some cases, parametric modelling or typological clustering is used to determine the impact of certain spatial variables, such as envelope exposure or orientation. However, the diversity and complexity of the actual urban fabric limits these models, as neither clustering nor parametric modelling can depict the specific urban setting around the observed buildings. Computing solar obstruction is particularly challenging since it involves spatial and temporal dynamics. The Litheum model uses a novel algorithm to calculate the obstruction angle of each building at different orientations. This information is stored in geographical features, which exponentially minimises the computation requirements in the energy server of the online platform.

EN 52016-1 contains simplified monthly and detailed hourly methods, which are described in the accompanying technical documents. Although subsequent studies have

questioned the accuracy of these methods, the guiding principle of the standard was to balance precision with flexibility and reproducibility. It was observed that this approach was convenient for large-scale urban modelling, since overly complex methods can compromise their applicability on a large scale. The Litheum model has adapted and translated the EN 52016 standard into Python code to enable hosting on the platform's energy server. The resulting tool was successfully tested in accordance with the standard's verification procedure.

The tool was tested in three pilot cases in Spain, covering a small town (Pontevedra), a mid-sized city (A Coruña), and a large capital city (Madrid). The objective was to deploy and test the platform gradually and receive feedback from user groups. This feedback was gathered through focus groups with planning teams and semi-structured interviews with city representatives and officials. It was found that size was not an issue other than requiring more computing time to process the base layer, particularly for calculating and storing the obstruction angles. The studies also revealed some inconsistencies in the cadastral cartography, which could be resolved with minor code adaptations. Additional functionalities were incorporated into the model following the feedback received, such as a solar control mode, which is particularly relevant in warm seasons and climates. Future work will involve expanding and testing the model in different climates worldwide.

The development and implementation of Litheum revealed several important insights. Firstly, integrating standardised energy calculation methods into user-friendly web tools is feasible and valuable in bridging the gap between complex models and practical planning and design applications. Secondly, accurate urban energy modelling requires the careful pre-processing of spatial data, particularly with regard to solar obstruction and envelope exposure. This proved to be computationally demanding, but essential for achieving robust results. Furthermore, the integration of Urban Climate Models has

become feasible due to modular structures and the availability of open-source applications. Thirdly, stakeholder feedback was instrumental in identifying usability gaps and prioritising feature development, thus confirming the importance of iterative co-design with end users. Finally, the model's scalability depends heavily on strategic simplifications and modular architecture, enabling adaptation across diverse urban contexts without compromising core accuracy.

References:

Aerts, D., Minnen, J., Glorieux, I., Wouters, I., & Descamps, F. (2014). A method for the identification and modelling of realistic domestic occupancy sequences for building energy demand simulations and peer comparison. *Building and Environment*, *75*, 67-78. https://doi.org/10.1016/j.buildenv.2014.01.021

Ahmed, K., Akhondzada, A., Kurnitski, J., & Olesen, B. (2017). Occupancy schedules for energy simulation in new prEN16798-1 and ISO/FDIS 17772-1 standards. *Sustainable Cities and Society*, *35*, 134-144. https://doi.org/10.1016/j.scs.2017.07.010

Ali, U., Shamsi, M. H., Hoare, C., Mangina, E., & O'Donnell, J. (2021). Review of urban building energy modeling (UBEM) approaches, methods and tools using qualitative and quantitative analysis. *Energy and Buildings*, *246*, 111073. https://doi.org/10.1016/j.enbuild.2021.111073

Álvarez, J. A., Rabuñal, J. R., García-Vidaurrázaga, D., Alvarellos, A., & Pazos, A. (2018). Modeling of Energy Efficiency for Residential Buildings Using Artificial Neuronal Networks. *Advances in Civil Engineering*, *2018*(1), 7612623. https://doi.org/10.1155/2018/7612623

Andersen, M., & De Boer, J. (2006). Goniophotometry and assessment of bidirectional photometric properties of complex fenestration systems. *Energy and Buildings*, *38*(7), 836-848. https://doi.org/10.1016/j.enbuild.2006.03.009

Ang, Y. Q., Berzolla, Z. M., Letellier-Duchesne, S., Jusiega, V., & Reinhart, C. (2022). UBEM.io: A web-based framework to rapidly generate urban building energy models for carbon reduction technology pathways. *Sustainable Cities and Society*, *77*, 103534. https://doi.org/10.1016/j.scs.2021.103534

ANSI/ASHRAE. (2014). *Standard 140 Standard Method of Test for the Evaluation of Building Energy Analysis Computer Programs*. https://codes.iccsafe.org/content/ASHRAE1402014P1

Arcas Abella, J., Pagès Ramon, A., Romero Gutiérrez, A., & Bilbao Figuero, A. (2018). *Aproximación a la demanda energética residencial para calefacción en España. Estudio para la ERESEE*. Ministerio de Fomento.

Baker, N., & Steemers, K. (2000). *Energy and environment in architecture: A technical design guide*. E&FN Spon.

Berthou, T., Stabat, P., Salvazet, R., & Marchio, D. (2014). Development and validation of a gray box model to predict thermal behavior of occupied office buildings. *Energy and Buildings*, *74*, 91-100. https://doi.org/10.1016/j.enbuild.2014.01.038

BRE. (1986). *Digest 310: Estimating daylight in buildings: Part 2*. Building Research Establishment.

BRE. (2009). *ClimateLite. Designing Low Carbon Buildings*. https://www.bre.co.uk/filelibrary/pdf/cap/Climate_Lite_Leaflet_Layout_1.pdf

Bueno, B., Norford, L., Hidalgo, J., & Pigeon, G. (2013). The urban weather generator. *Journal of Building Performance Simulation*, *6*(4), 269-281. https://doi.org/10.1080/19401493.2012.718797

Bueno, B., Norford, L., Pigeon, G., & Britter, R. (2012). A resistance-capacitance network model for the analysis of the interactions between the energy performance of buildings and the urban climate. *Building and Environment*, *54*, 116-125. https://doi.org/10.1016/j.buildenv.2012.01.023

Cadima, P., & Rodríguez Álvarez, J. (2021). O contexto europeu da reabilitação de edifícios. En *Edifício ambiental* (pp. 417-451). Oficina de Textos.

Chen, Y., Hong, T., & Piette, M. A. (2017). *Automatic Generation and Simulation of Urban Building Energy Models Based on City Datasets for City-Scale Building Retrofit Analysis*. Lawrence Berkeley National Laboratory.

Ciclica. (2023). *Urban3R* (Versión 1.0) [Software]. Ministerio de Vivienda y Agenda Urbana. Gobierno de España. https://urban3r.es/

De Luca, G., Bianco Mauthe Degerfeld, F., Ballarini, I., & Corrado, V. (2022). Improvements of simplified hourly models for the energy assessment of buildings: The application of EN ISO 52016 in Italy. *Energy Reports*, *8*, 7349-7359. https://doi.org/10.1016/j.egyr.2022.05.120

DEA. (2018). *2018 Implementing the Energy Performance of Buildings Directive (EPBD). Country Reports*.

Dobias, T. (2023). *PyQGIS Developer Cookbook v.3.34*. QGIS. https://docs.qgis.org/3.34/en/docs/pyqgis_developer_cookbook/index.html

Dogan, T., & Reinhart, C. (2017). Shoeboxer: An algorithm for abstracted rapid multi-zone urban building energy model generation and simulation. *Energy and Buildings*, *140*, 140-153. https://doi.org/10.1016/j.enbuild.2017.01.030

El Kontar, R., Polly, B., Charan, T., Fleming, K., Moore, N., Long, N., & Goldwasser, D. (2020). *URBANopt: An Open-Source Software Development Kit for Community and Urban District Energy Modeling: Preprint*. https://www.osti.gov/biblio/1677416

EU Science Hub. (2024). *Photovoltaic Geographical Information System (PVGIS)* [PVGIS]. https://joint-research-centre.ec.europa.eu/photovoltaic-geographical-information-system-pvgis_en

European Commission. (2020). A renovation wave for Europe—Greening our buildings, creating jobs, improving lives. *Official Journal of the European Union*, 26.

Fabre, A., Thomas, R., Duplessis, B., Tran, C.-T., & Stabat, P. (2018). Dynamic modeling for evaluation of triple-pipe configuration potential in geothermal district heating networks. *Energy Conversion and Management*, *173*, 461-469. https://doi.org/10.1016/j.enconman.2018.07.087

Ferrando, M., Causone, F., Hong, T., & Chen, Y. (2020). Urban building energy modeling (UBEM) tools: A state-of-the-art review of bottom-up physics-based approaches. *Sustainable Cities and Society*, *62*, 102408. https://doi.org/10.1016/j.scs.2020.102408

Flask (Versión 3.1.1). (2024). [Software]. Pallets. https://flask.palletsprojects.com/en/stable/

Fonseca, J. A., & Schlueter, A. (2015). Integrated model for characterization of spatiotemporal building energy consumption patterns in neighborhoods and city districts. *Applied Energy*, *142*, 247-265. https://doi.org/10.1016/j.apenergy.2014.12.068

García Cepeda, F. (2006). Control de Calidad en el Área de Cartografía Informatizada de la Dirección General del Catastro. *CT:Catastro*, *56*, 7-26.

Gómez-Gil, M., Sesana, M. M., Salvalai, G., Espinosa-Fernández, A., & López-Mesa, B. (2023). The Digital Building Logbook as a gateway linked to existing national data sources: The cases of Spain and Italy. *Journal of Building Engineering*, *63*, 105461. https://doi.org/10.1016/j.jobe.2022.105461

Groth, C. C., & Lokmanhekim, M. (1969). *Shadow - A New Technique for the Calculation of Shadow Shapes and Areas by Digital Computer*. *2*, 471-474.

Hallik, J., Arumägi, E., Pikas, E., & Kalamees, T. (2024). Comparative assessment of simple and detailed energy performance models for urban energy modelling based on digital twin and statistical typology database for the renovation of existing building stock. *Energy and Buildings*, *323*, 114775. https://doi.org/10.1016/j.enbuild.2024.114775

Harb, H., Boyanov, N., Hernandez, L., Streblow, R., & Müller, D. (2016). Development and validation of grey-box models for forecasting the thermal response of occupied buildings. *Energy and Buildings*, *117*, 199-207. https://doi.org/10.1016/j.enbuild.2016.02.021

Harish, V. S. K. V., & Kumar, A. (2016). Reduced order modeling and parameter identification of a building energy system model through an optimization routine. *Applied Energy*, *162*, 1010-1023. https://doi.org/10.1016/j.apenergy.2015.10.137

Hirst, E. (1978). A model of residential energy use. *SIMULATION*, *30*(3), 69-74. https://doi.org/10.1177/003754977803000301

Hong, T., Langevin, J., Luo, N., & Sun, K. (2020). Developing quantitative insights on building occupant behaviour: Supporting modelling tools and datasets. En *Energy and Behaviour* (pp. 283-319). Elsevier. https://doi.org/10.1016/B978-0-12-818567-4.00012-0

Huang, J., Jones, P., Zhang, A., Peng, R., Li, X., & Chan, P. (2020). Urban Building Energy and Climate (UrBEC) simulation: Example application and field evaluation in Sai Ying Pun, Hong Kong. *Energy and Buildings*, *207*, 109580. https://doi.org/10.1016/j.enbuild.2019.109580

ISO. (2008). *ISO 13790:2008. Energy performance of buildings—Calculation of energy use for space heating and cooling*.

ISO. (2016). *ISO 52016_1 Bestest ClimData* [Dataset]. ISO Standards Maintenance Portal. https://standards.iso.org/iso/52016/-1/ed-1/

ISO. (2017a). *ISO 13789:2017. Thermal performance of buildings. Transmission and ventilation heat transfer coefficients. Calculation method*.

ISO. (2017b). *ISO 52016-1:2017. Energy performance of buildings—Energy needs for heating and cooling, internal temperatures and sensible and latent heat loads. Part 1: Calculation procedures*.

ISO. (2017c). *ISO 52016-1:2017. Energy performance of buildings—Energy needs for heating and cooling, internal temperatures and sensible and latent heat loads. Part 2: Explanation and justification of ISO 52016-1 and ISO 52017-1*.

ISO. (2017d). *ISO 52017-1:2017. Energy performance of buildings. Sensible and latent heat loads and internal temperatures. Part 1: Generic calculation procedures*.

Jimeno Fonseca, Daren Thomas, Reynold Mok, Shanshan Hsieh, Bhargava Krishna Sreepathi, Gabriel Happle, Lennart Rogenhofer, Mathias Niffeler, Zhongming Shi, Martín Mosteiro Romero, Jack-Hawthorne, khayatian, Emanuel Riegelbauer, lguilhermers, Amedeo Ceruti, Bo Lie Ong, orenkiwi, jarunan, Maryam MeshkinKiya, … The Gitter Badger. (2024). *architecture-building-systems/CityEnergyAnalyst: CityEnergyAnalyst v4.0.0-alpha.4* (Versión v4.0.0-alpha.4) [Software]. Zenodo. https://doi.org/10.5281/ZENODO.598221

Jones, P. J, Williams, J., & Lannon, S. (1998, diciembre). *An energy and environmental prediction tool for planning sustainability in cities*.

Kamel, E. (2022). A Systematic Literature Review of Physics-Based Urban Building Energy Modeling (UBEM) Tools, Data Sources, and Challenges for Energy Conservation. *Energies*, *15*(22), 8649. https://doi.org/10.3390/en15228649

Kastner, P., & Dogan, T. (2024). Towards Auto-Calibrated UBEM Using Readily Available, Underutilized Urban Data: A Case Study for Ithaca, NY. *Energy and Buildings*, *317*, 114286. https://doi.org/10.1016/j.enbuild.2024.114286

Keirstead, J. (2013). Benchmarking urban energy efficiency in the UK. *Energy Policy*, *63*, 575-587. https://doi.org/10.1016/j.enpol.2013.08.063

Kristensen, M. H., Hedegaard, R. E., & Petersen, S. (2018). Hierarchical calibration of archetypes for urban building energy modeling. *Energy and Buildings*, *175*, 219-234. https://doi.org/10.1016/j.enbuild.2018.07.030

Li, X., & Yao, R. (2021). Modelling heating and cooling energy demand for building stock using a hybrid approach. *Energy and Buildings*, *235*, 110740. https://doi.org/10.1016/j.enbuild.2021.110740

Li, X., Zhou, Y., Yu, S., Jia, G., Li, H., & Li, W. (2019). Urban heat island impacts on building energy consumption: A review of approaches and findings. *Energy*, *174*, 407-419. https://doi.org/10.1016/j.energy.2019.02.183

Li, Y., O'Neill, Z., Zhang, L., Chen, J., Im, P., & DeGraw, J. (2021). Grey-box modeling and application for building energy simulations—A critical review. *Renewable and Sustainable Energy Reviews*, *146*, 111174. https://doi.org/10.1016/j.rser.2021.111174

Lundström, L., Akander, J., & Zambrano, J. (2019). Development of a Space Heating Model Suitable for the Automated Model Generation of Existing Multifamily Buildings—A Case Study in Nordic Climate. *Energies*, *12*(3), 485. https://doi.org/10.3390/en12030485

Maiullari, D., Mosteiro-Romero, M., & Pijpers-van Esch, M. (2018). Urban Microclimate and Energy Performance: An Integrated Simulation Method. En E. Ng, S. Fong, & C. Ren (Eds.), *PLEA 2018: Smart and Healthy Within the Two-Degree Limit:*

Proceedings of the 34th International Conference on Passive and Low Energy Architecture: Volume 1 (pp. 384-389). PLEA 2018.

Marsh, A. (2004). *Non-Uniformity in Incident Solar Radiation over the Facades of High Rise Buildings*. *1*, 19-22.

Mazzarella, L., Scoccia, R., Colombo, P., & Motta, M. (2020). Improvement to EN ISO 52016-1:2017 hourly heat transfer through a wall assessment: The Italian National Annex. *Energy and Buildings*, *210*, 109758. https://doi.org/10.1016/j.enbuild.2020.109758

McNeil, A., Jonsson, C. J., Appelfeld, D., Ward, G., & Lee, E. S. (2013). A validation of a ray-tracing tool used to generate bi-directional scattering distribution functions for complex fenestration systems. *Solar Energy*, *98*, 404-414. https://doi.org/10.1016/j.solener.2013.09.032

Mendes, V. F., Cruz, A. S., Gomes, A. P., & Mendes, J. C. (2024). A systematic review of methods for evaluating the thermal performance of buildings through energy simulations. *Renewable and Sustainable Energy Reviews*, *189*, 113875. https://doi.org/10.1016/j.rser.2023.113875

NREL. (2014). *DryCold Weather File (epw)* [Dataset]. GitHub. https://github.com/NREL/EnergyPlus/blob/develop/weather/drycold.epw

NREL, ANL, LBNL, ORNL, & PNNL. (2023). *OpenStudio*® (Versión 3.9.0) [Software]. U.S. Department of Energy, Office of Energy Efficiency and Renewable Energy. https://openstudio.net

Pasandi, L., Qian, Z., Woo, W. L., & Palacin, R. (2024). A comprehensive review of applications and feedback impact of microclimate on building operation and energy. *Building and Environment*, *263*, 111855. https://doi.org/10.1016/j.buildenv.2024.111855

Pili, S., Desogus, G., & Melis, D. (2018). A GIS tool for the calculation of solar irradiation on buildings at the urban scale, based on Italian standards. *Energy and Buildings*, *158*, 629-646. https://doi.org/10.1016/j.enbuild.2017.10.027

PostgreSQL Global Development Group. (2024). *PostgreSQL* (Versión 17.2) [Software]. https://www.postgresql.org

Ramallo-González, A. P., Eames, M. E., & Coley, D. A. (2013). Lumped parameter models for building thermal modelling: An analytic approach to simplifying complex multi-layered constructions. *Energy and Buildings*, *60*, 174-184. https://doi.org/10.1016/j.enbuild.2013.01.014

Ratti, C., Baker, N., & Steemers, K. (2005). Energy consumption and urban texture. *Energy and Buildings*, *37*(7), 762-776. https://doi.org/10.1016/j.enbuild.2004.10.010

Ratti, C., Robinson, D., Baker, N., & Steemers, K. (2000). LT Urban. The energy modeling of urban form. *Architecture City Environment: Proceedings of PLEA 2000, Cambridge, UK 2-5 July 2000*, 660-666.

Reinhart, C., Dogan, T., Jakubiec, A., Rakha, T., & Sang, A. (2013, agosto 28). *Umi – An Urban Simulation Environment For Building Energy Use, Daylighting And Walkability*. 2017 Building Simulation Conference. https://doi.org/10.26868/25222708.2013.1404

Reinhart, C. F., & Cerezo Davila, C. (2016). Urban building energy modeling – A review of a nascent field. *Building and Environment*, *97*, 196-202. https://doi.org/10.1016/j.buildenv.2015.12.001

Richardson, I., Thomson, M., & Infield, D. (2008). A high-resolution domestic building occupancy model for energy demand simulations. *Energy and Buildings*, *40*(8), 1560-1566. https://doi.org/10.1016/j.enbuild.2008.02.006

Ritchie, H. (2020). Sector by sector: Where do global greenhouse gas emissions come from? *Our World in Data*.

Robinson, D. (Ed.). (2011). *Computer modelling for sustainable urban design: Physical principles, methods and applications*. Earthscan.

Robinson, D., Campbell, N., Gaiser, W., Kabel, K., Le-Mouel, A., Morel, N., Page, J., Stankovic, S., & Stone, A. (2007). SUNtool – A new modelling paradigm for simulating and optimising urban sustainability. *Solar Energy*, *81*(9), 1196-1211. https://doi.org/10.1016/j.solener.2007.06.002

Rodríguez-Álvarez, J. (2014). *Planning cities for the post-carbon age: A metabolic analysis of the urban form* [University of A Coruna]. http://hdl.handle.net/2183/11927

Rodríguez-Álvarez, J. (2016). Urban Energy Index for Buildings (UEIB): A new method to evaluate the effect of urban form on buildings' energy demand. *Landscape and Urban Planning*, *148*, 170-187. https://doi.org/10.1016/j.landurbplan.2016.01.001

Rodríguez-Álvarez, J. (2023). Urban Building Energy Modelling for the Renovation Wave: A Bespoke Approach Based on EPC Databases. *Buildings*, *13*(7), 1636. https://doi.org/10.3390/buildings13071636

Rodríguez-Álvarez, J., & Alvaredo-López, N. (2023). Interactive energy mapping for effective plans and policies. A user-centered UBEM approach. *EESAP14 International Conference 2023, 4-5 October, Donostia – San Sebastián. Proceedings book*, 41-51. http://hdl.handle.net/2183/37293

Rouchier, S., Rabouille, M., & Oberlé, P. (2018). Calibration of simplified building energy models for parameter estimation and forecasting: Stochastic versus deterministic modelling. *Building and Environment*, *134*, 181-190. https://doi.org/10.1016/j.buildenv.2018.02.043

Salvalai, G., Zhu, Y., & Maria Sesana, M. (2024). From building energy modeling to urban building energy modeling: A review of recent research trend and simulation tools. *Energy and Buildings*, *319*, 114500. https://doi.org/10.1016/j.enbuild.2024.114500

Santamouris, M. (2014). On the energy impact of urban heat island and global warming on buildings. *Energy and Buildings*, *82*, 100-113. https://doi.org/10.1016/j.enbuild.2014.07.022

Santamouris, M., Cartalis, C., Synnefa, A., & Kolokotsa, D. (2015). On the impact of urban heat island and global warming on the power demand and electricity consumption of buildings—A review. *Energy and Buildings*, *98*, 119-124. https://doi.org/10.1016/j.enbuild.2014.09.052

SEC. (2024). *Cadastre Digital Platform* [Dataset]. Cadastral Database. https://www.sedecatastro.gob.es/Accesos/SECAccDescargaDatos.aspx#

Seo, J., Kim, S., Lee, S., Jeong, H., Kim, T., & Kim, J. (2022). Data-driven approach to predicting the energy performance of residential buildings using minimal input data. *Building and Environment*, *214*, 108911. https://doi.org/10.1016/j.buildenv.2022.108911

Sezer, N., Yoonus, H., Zhan, D., Wang, L. (Leon), Hassan, I. G., & Rahman, M. A. (2023). Urban microclimate and building energy models: A review of the latest progress in coupling strategies. *Renewable and Sustainable Energy Reviews*, *184*, 113577. https://doi.org/10.1016/j.rser.2023.113577

Sola, A., Corchero, C., Salom, J., & Sanmarti, M. (2020). Multi-domain urban-scale energy modelling tools: A review. *Sustainable Cities and Society*, *54*, 101872. https://doi.org/10.1016/j.scs.2019.101872

Soriano, P., Raga, F., García de Marina, L., & Pérez, F. (2024). *Spanish_Inspire_Catastral_Downloader* (Versión 2.1) [Software]. https://github.com/sigdeletras/Spanish_Inspire_Catastral_Downloader

Spring Framework. (2024). [Software]. Broadcom Inc. https://spring.io/projects/spring-framework

Swan, L. G., & Ugursal, V. I. (2009). Modeling of end-use energy consumption in the residential sector: A review of modeling techniques. *Renewable and Sustainable Energy Reviews*, *13*(8), 1819-1835. https://doi.org/10.1016/j.rser.2008.09.033

Szcześniak, J. T., Ang, Y. Q., Letellier-Duchesne, S., & Reinhart, C. F. (2022). A method for using street view imagery to auto-extract window-to-wall ratios and its relevance for urban-level daylighting and energy simulations. *Building and Environment*, *207*, 108108. https://doi.org/10.1016/j.buildenv.2021.108108

Teller, J., & Azar, S. (2001). Townscope II—A computer system to support solar access decision-making. *Solar Energy*, *70*(3), 187-200. https://doi.org/10.1016/S0038-092X(00)00097-9

Turégano, J., & Hernández, M. (2008). *Urban design with sustainable energy criteria. Computer application for municipalities. The Ursos Project*.

U.S. Department of Energy. (2024). *Engineering Reference. EnergyPlus™ Version 24.2.0 Documentation*. https://energyplus.net/assets/nrel_custom/pdfs/pdfs_v24.2.0/EngineeringReference.pdf

van Dijk, D. (2021). *Conversion from TMY data set to input for (EN) ISO 52010-1* [Software]. EPB Center. https://epb.center/support/documents/tmy-iso-52010-1_conversion/

Van Dijk, D., & Hogeling, J. (2019). The new EN ISO 52000 family of standards to assess the energy performance of buildings put in practice. *E3S Web of Conferences*, *111*, 04047. https://doi.org/10.1051/e3sconf/201911104047

Van Dijk, D., Spiekman, M., & Hoes-Van Oeffelen, L. (2016). EPB standard EN ISO 52016: Calculation of the building's energy needs for heating and cooling, internal temperatures and heating and cooling load. *REHVA Journal*, *53*(5). https://www.rehva.eu/rehva-journal/detail/05-2016

Van Dijk, D., Spiekman, M., Van Orshoven, D., & Plokker, W. (2015). Subset of EPB standards on the energy use and the thermal performance of buildings and building elements. *REHVA Journal*, *1*, 6-16.

Villanueva-Díaz, C., Álvarez-Sanz, M., Campos-Celador, Á., & Terés-Zubiaga, J. (2024). The Open Data Potential for the Geospatial Characterisation of Building Stock on an Urban Scale: Methodology and Implementation in a Case Study. *Sustainability*, *16*(2), 652. https://doi.org/10.3390/su16020652

Walsh, A., Cóstola, D., & Labaki, L. C. (2017). Review of methods for climatic zoning for building energy efficiency programs. *Building and Environment*, *112*, 337-350. https://doi.org/10.1016/j.buildenv.2016.11.046

Walton, G. N. (1978). The Application of Homogeneous Coordinates to Shadowing Calculations. *ASHRAE Transactions*, *84*(2).

Wang, S., & Xu, X. (2006). Simplified building model for transient thermal performance estimation using GA-based parameter identification. *International Journal of Thermal Sciences*, *45*(4), 419-432. https://doi.org/10.1016/j.ijthermalsci.2005.06.009

Wang, Z., & Chen, Y. (2019). Data-driven modeling of building thermal dynamics: Methodology and state of the art. *Energy and Buildings*, *203*, 109405. https://doi.org/10.1016/j.enbuild.2019.109405

Wang, Z., Chen, Y., & Li, Y. (2019). Development of RC model for thermal dynamic analysis of buildings through model structure simplification. *Energy and Buildings*, *195*, 51-67. https://doi.org/10.1016/j.enbuild.2019.04.042

Yang, J., Wang, H., Cheng, L., Gao, Z., & Xu, F. (2024). A review of resistance–capacitance thermal network model in urban building energy simulations. *Energy and Buildings*, *323*, 114765. https://doi.org/10.1016/j.enbuild.2024.114765

You, E. (2024). *Vue.js* (Versión v.3.5.13) [Software]. VoidZero. https://vuejs.org/

Zakula, T., Badun, N., Ferdelji, N., & Ugrina, I. (2021). Framework for the ISO 52016 standard accuracy prediction based on the in-depth sensitivity analysis. *Applied Energy*, *298*, 117089. https://doi.org/10.1016/j.apenergy.2021.117089

Zarrella, A., Prataviera, E., Romano, P., Carnieletto, L., & Vivian, J. (2020). Analysis and application of a lumped-capacitance model for urban building energy modelling. *Sustainable Cities and Society*, *63*, 102450. https://doi.org/10.1016/j.scs.2020.102450

Zhuo, X., Tian, J., & Häfele, K.-H. (2023). Direct Window-to-Wall Ratio Prediction Using Deep Learning Approaches. *2023 Joint Urban Remote Sensing Event (JURSE)*, 1-4. https://doi.org/10.1109/JURSE57346.2023.10144162